Research Paper

Retromer in Osteoblasts Interacts With Protein Phosphatase 1 Regulator Subunit 14C, Terminates Parathyroid Hormone's Signaling, and Promotes Its Catabolic Response

CrossMark

Lei Xiong [a,b], Wen-Fang Xia [a,b,c], Fu-Lei Tang [a,b], Jin-Xiu Pan [a,b], Lin Mei [a,b], Wen-Cheng Xiong [a,b,*]

[a] Department of Neuroscience & Regenerative Medicine, Department of Neurology, Medical College of Georgia, Augusta, GA 30912, United States
[b] Charlie Norwood VA Medical Center, Augusta, GA 30912, United States
[c] Department of Endocrinology, Union Hospital, Tongji Medical College, Huazhong University of Science and Technology, Wuhan 430022, China

ARTICLE INFO

ABSTRACT

Parathyroid hormone (PTH) plays critical, but distinct, roles in bone remodeling, including bone formation (anabolic response) and resorption (catabolic response). Although its signaling and function have been extensively investigated, it just began to be understood how distinct functions are induced by PTH activating a common receptor, the PTH type 1 receptor (PTH1R), and how PTH1R signaling is terminated. Here, we provide evidence for vacuolar protein sorting 35 (VPS35), a major component of retromer, in regulating PTH1R trafficking, turning off PTH signaling, and promoting its catabolic function. VPS35 is expressed in osteoblast (OB)-lineage cells. VPS35-deficiency in OBs impaired PTH$_{(1–34)}$-promoted PTH1R translocation to the *trans*-Golgi network, enhanced PTH$_{(1–34)}$-driven signaling, and reduced PTH$_{(1–34)}$'s catabolic response in culture and in mice. Further mechanical studies revealed that VPS35 interacts with not only PTH1R, but also protein phosphatase 1 regulatory subunit 14C (PPP1R14C), an inhibitory subunit of PP1 phosphatase. PPP1R14C also interacts with PTH1R, which is necessary for the increased endosomal PTH1R signaling and decreased PTH$_{(1–34)}$'s catabolic response in VPS35-deficient OB-lineage cells. Taken together, these results suggest that VPS35 deregulates PTH1R-signaling likely by its interaction with PTH1R and PPP1R14C. This event is critical for the control of PTH$_{(1–34)}$-signaling dynamics, which may underlie PTH-induced catabolic response and adequate bone remodeling.

Published by Elsevier B.V. This is an open access article under the CC BY-NC-ND license (http://creativecommons.org/licenses/by-nc-nd/4.0/).

1. Introduction

VPS35 is a critical component of the cargo-recognition sub-complex of retromer that contains VPS26, VPS29, and VPS35. Clinically, VPS35/ retromer dysfunction is a risk factor for pathogenesis of neurodegenerative disorders, including Alzheimer's disease (AD) and Parkinson's disease (PD) (Dhungel et al., 2015; Muhammad et al., 2008; Small et al., 2005; Small and Petsko, 2015; Tang et al., 2015a; Tang et al., 2015b; Vilarino-Guell et al., 2011; Wen et al., 2011; Zimprich et al., 2011). Intriguingly, in addition to neurodegenerative pathology, AD patients frequently have lower bone-mass and higher hip fracture rate, compared with the same age normal population(Luckhaus et al., 2009; Melton et al., 1994; Sato et al., 1998; Sato et al., 2004; Tan et al., 2005; Tysiewicz-Dudek et al., 2008); and some PD patients have Paget disease of the bone, a chronic disorder caused by the excessive bone resorption and formation (Helfrich and Hocking, 2008; Reid, 2012). In addition to VPS35, several newly identified AD risk genes/loci (e.g., TREM2, and PYK2) encode proteins critical for osteoclastic

activation and bone homeostasis (Duong et al., 1998; Guerreiro et al., 2013; Paloneva et al., 2003; Pfaff and Jurdic, 2001; Singaraja, 2013; Small et al., 2005; Wang et al., 2003). Thus, increasing evidence from clinical and genetic studies supports a degree of co-morbidity of these disorders. However, very few studies are available to address their relationship.

Cell biologically, the retromer complex is essential for retrieval of transmembrane proteins or receptors from endosome-to-Golgi apparatus (Bonifacino and Hurley, 2008; McGough and Cullen, 2011; Seaman et al., 2013; Seaman et al., 1997). A growing list of retromer cargos has been identified, such as VPS10/sortilin/SorLA family proteins(Seaman, 2005), cation-independent M6P receptor (CI-M6PR) (Seaman, 2004), mammalian iron transporter DMT1(Tabuchi et al., 2010), amyloid precursor protein (APP) (Vieira et al., 2010), APP processing β1 secretase (BACE1) (Wen et al., 2011), *Caenorhabditis elegans* phagocytosis receptor Ced1(Chen et al., 2010), receptor activator of nuclear factor kappa-B (RANK) (Xia et al., 2013b), and seven transmembrane receptors such as Wntless (Belenkaya et al., 2008; Pan et al., 2008; Yang et al., 2008), β2-adrenergic receptor (Choy et al., 2014; Temkin et al., 2011), and PTH1R (type 1 receptor for parathyroid hormone) (Feinstein et al., 2011). Thus, VPS35/retromer is likely to be involved in various cellular functions or processes via its regulation of different cargos.

Several lines of evidence implicate VPS35/retromer in bone remodeling or bone homeostasis. First, VPS35 is highly expressed in both OB- and OC-lineage cells (Xia et al., 2013b). Second, VPS35/retromer's cargos, such as PTH1R, Wntless, and RANK, are critical for bone remodeling or bone homeostasis (Cheloha et al., 2015; Coudreuse et al., 2006; Eaton, 2008; Feinstein et al., 2011; Franch-Marro et al., 2008; Xia et al., 2013b; Zhong et al., 2012). Third, young adult Vps35-heterozygote (Vps35$^{+/m}$) mice display lower bone-mass with reduced bone formation and increased bone resorption (Xia et al., 2013b). RANKL (receptor activator of nuclear factor kappa-B ligand) signaling is increased and sustained in Vps35-deficient bone marrow macrophages (BMMs), resulting in an increased OC formation and bone resorption (Xia et al., 2013b). While this study has pointed to the importance of hyper-resorptive OCs for the osteoporotic deficit in Vps35$^{+/m}$ mice, the reduced bone formation may also have a critical role in this deficit. However, it remains unclear the exact role of VPS35/retromer and the functional significance of VPS35/retromer regulation of PTH1R in OB-lineage cells.

PTH1R, a receptor of PTH, is an essential regulator of not only calcium–phosphorus metabolism, but also bone remodeling (Cheloha et al., 2015; Vilardaga et al., 2012). Intermittent treatment with human recombinant PTH$_{(1-34)}$ promotes recruitments of both OB and OC and a net bone-gain; but continued treatment leads to more OC activation with a net bone-loss (Cheloha et al., 2015; Vilardaga et al., 2012). It is of considerable interest to investigate how PTH$_{(1-34)}$ activation of PTH1R results in such complex metabolic effects. PTH$_{(1-34)}$ activation of PTH1R stimulates adenylate cyclase (AC)-mediated cAMP production by Gαs and increases PLC-mediated [Ca^{2+}]i (cytosolic free Ca^{2+} concentration) by Gαq (Cheloha et al., 2015; Vilardaga et al., 2012). These G-protein mediated signaling events, so called cell surface or canonical GPCR (G-protein coupled receptor) signaling, contribute to the complex metabolic effects induced by PTH (Vilardaga et al., 2012; Whalen et al., 2011). However, recent studies have found that β-arrestin serves as a multifunctional scaffolding protein linking the PTH1R to signaling endosomes independent of the cell surface or canonical GPCR pathway, and thus called endosomal or non-canonical GPCR signaling, which are also important for the complex metabolic effects (Vilardaga et al., 2012; Whalen et al., 2011). Exactly how both PTH-induced cell surface and endosomal signaling events are involved in the complex metabolic functions, and how both pathways are regulated and/or terminated, remain poorly understood.

Here, we provide evidence that VPS35 in OB-lineage cells is necessary for maintaining bone mass. Mice that selectively knock out VPS35 in mature OBs, Vps35$^{Ocn-Cre}$, as that of Vps35$^{+/-}$, displayed reduced bone-mass. However, PTH$_{(1-34)}$ treatments diminished such an osteoporotic deficit in both Vps35$^{Ocn-Cre}$ and Vps35$^{+/-}$ mutant alleles. In addition, a more dramatic trabecular bone-gain response to PTH$_{(1-34)}$ was detected in both Vps35 mutant alleles, as compared with that of control mice. The increased bone-gain response might be due to an impaired PTH$_{(1-34)}$-driven catabolic response or bone resorption. Further mechanistic studies showed that VPS35 in OB-lineage cells is required to turn off PTH$_{(1-34)}$-signaling. Such a negative regulation of PTH$_{(1-34)}$ signaling (in particular, the endosomal signaling) is likely due to VPS35 promotion of PTH$_{(1-34)}$-induced PTH1R translocation to the Golgi apparatus as well as VPS35 interaction with an inhibitor of PP1 phosphatase, PPP1R14C. This negative regulation of PTH$_{(1-34)}$-driven endosomal signaling appeared to be crucial for PTH$_{(1-34)}$-induction of catabolic response. Taken together, these results demonstrate a critical role for osteoblastic VPS35 to de-regulate PTH1R signaling, reveal a mechanism underlying VPS35 suppression of PTH1R-driven endosomal signaling, and provide insights into PTH$_{(1-34)}$-induced catabolic response and adequate bone remodeling.

2. Materials and Methods

2.1. Reagents and Animals

Rabbit polyclonal anti-VPS35 antibody was generated using the antigen of GST-VPS35D1 fusion protein as described previously (Wen et al., 2011). Rabbit polyclonal antibodies, including pCREB (#9198S, Cell Signaling), pErk1/2 (#4370S, Cell Signaling), Erk1/2 (#9102S, Cell Signaling), pAkt (#4060P, Cell Signaling), Akt (#4691S, Cell Signaling), pSmad1/5/8 (Cell Signaling), PTH1R (PRB-630P-100, Covance), mCherry (ab183628, Abcam), EEA1 (ab2900, Abcam), PPP1R14A (ARP63944, Aviva Systems Biology), and PPP1R14C (AP10151b, Abgent) antibodies, were used. Mouse monoclonal antibodies, including Flag (F1804, Sigma), V5 (V8012, Sigma), GM130 (BD Bioscience), and Rat anti-LAMP1 (DSHB) antibodies were used. Secondary antibodies were purchased from Jackson ImmunoResearch Laboratories, Inc. PTH$_{(1-34)}$ (human) was obtained from Bachem (H-4835). 1α, 25-Dihydroxyvitamin D3 and Forskolin was obtained from SIGMA (D1530 and F6886). Other chemicals and reagents used in this study were of analytical grade.

Vps35$^{+/-}$ mice (heterozygotes of Vps35 mutant mice) are generated by injection of mutant embryonic stem (ES) cells obtained from Bay Genomics as described previously (Wen et al., 2011). Vps35$^{f/f}$ mice were generated as described previously (Tang et al., 2015b). The Ocn-Cre mice were kindly provided by Dr. Tom Clemens (Johns Hopkins Medical School). Vps35$^{Ocn-Cre}$ mice were generated by crossing Vps35$^{f/f}$ with Ocn-Cre mice. Mice in C57BL6 background (>10 generations) were maintained on a standard rodent diet (Harlan Tekled S-2335). Control littermates were processed in parallel for each experiment. The Vps35 mutation was confirmed by genotyping using polymerase chain reactions (PCR) and by Western blot analysis as described previously (Wen et al., 2011) (Tang et al., 2015b). All experimental procedures were approved by the Institutional Animal Care and Use Committee at Augusta University (previously called Georgia Regents University), according to US National Institutes of Health guidelines.

2.2. Plasmids and Lentiviruses

The miRNA-Vps35 expression vector was generated by the BLOCK-iT Lentiviral miR RNA expression System (Invitrogen, Carlsbad, CA) according to the manufacturer's instruction as previously described (Liu et al., 2012; Wang et al., 2012; Wen et al., 2011; Xia et al., 2013b; Zhu et al., 2007). The target sequences, 5′-AGGTGTAAATGTGGAACGTTA-3′ (for miRNA-Vps35), 5′-GGTACATCTATTTCTATGAAA-3′ (for shRNA-Vps35) and 5′-GCTGCGAGGAAGAAGAAATGC-3′(for shRNA-PPP1R14C) were designed using web-based Block-iT program (Invitrogen) and subcloned into pcDNA 6.2-GW/EmGFP-miR (Invitrogen) and pLV-shRNA (Biosettia) vectors, respectively. The PTH1R-mCherry expression plasmid was generated by fusion of the mCherry to the C-terminus of the RT-PCR amplified homo PTH1R (NM_000316, remove the stop codon, include signal peptide, 1779 bp) in a mammalian expression vector under control of the CAG promoter. PPP1R14C-V5 and GST-PPP1R14C plasmids were purchased from DNASU (HsCD00435544 and HsCD00734708). The authenticity of all constructs was verified by DNA sequencing.

The lentivirus was packaged by co-transfection of pLV-shRNA-Vps35 or pLV-shRNA-PPP1R14C with virus packaging plasmids into human embryonic kidney (HEK) 293 T cells using the PEI transfection method. In brief, 15 μg DNA mixture (7.5 μg pLV-shRNA-Vps35 or pLV-shRNA-PPP1R14C and 7.5 μg of pVSVG, PLP1, and PLP2, each at 2.5 μg, for one 100-mm dish) were prepared in serum-free DMEM, 7.5 μl PEI was added to the diluted DNA and mix immediately by vortexing or pipetting. The volume of PEI used is based on a 3:1 ratio of PEI (μg): total DNA (μg). The DNA/PEI mixture was added to cells after incubation 20 min at room temperature. 48 h after transfection, the viral supernatants were harvested and concentrated by centrifugation (25,000 rpm for 90 min at 4 degree).

2.3. PTH$_{(1-34)}$ Treatments

For in vivo experiments, P50 old Vps35$^{+/+}$ and Vps35$^{+/-}$ male mice or control (Vps35$^{f/f}$) and Vps35$^{Ocn-cre}$ mice were administered once daily injection of hPTH$_{(1-34)}$ 50 μg/Kg, or vehicle (0.9% sodium chloride),

5 days per week for a total of 5 weeks. Mice were sacrificed 24 h after the last injection. The serum and bone samples were collected.

For in vitro experiments, 100 nM PTH$_{(1-34)}$ was added to the growth medium at every medium change. For cell signaling and immunofluorescence staining experiments, cells were serum starved overnight and stimulated with PTH$_{(1-34)}$ for indicated time in the figure legend.

2.4. In Vitro BMSC Culture, Cell Line Culture and Transient Transfection

Whole bone marrow cells were flushed from long bones of WT and Vps35$^{+/m}$ mice and plated on 100 mm tissue culture plates in DMEM containing 10% fetal bovine serum (FBS), 1% penicillin/streptomycin (P/S). Plates were replaced with fresh culture medium every 3 days. After 7 days, passaging cells by trypsin digestion, $1 * 10^4/cm^2$ were plated for PTH treatment experiments.

MC3T3-E1 cells were maintained in Dulbecco modified Eagle medium supplemented with 10% fetal calf serum, and 100 units/ml of penicillin G and streptomycin (Gibco). For examining PTH signaling experiments, cells was infected with lentiviruses expressing scramble control (GFP), shRNA-Vps35 (BFP or GFP) or shRNA-PPP1R14C (GFP) for 1 week and purified by Fluorescent activated cell sorting (FACS). The fluorescence-positive cells (GFP+ cells for Scramble control or shRNA-PPP1R14C; BFP+ cells for shRNA-Vps35; both GFP+ and BFP+ cells for shRNA-Vps35 + shRNA-PPP1R14C or shRNA-Vps35 + Scramble control) were cultured and used for experiments. For transfection, cells were plated at a density of 10^6 cells per 10-cm culture dish and allowed to grow for 12 h before transfection using Lipofectamine™ 2000 (Invitrogen). 48 h after transfection, cells were subjected to immunostaining analysis.

2.5. Osteoclast Precursors-osteoblast Co-cultures Assay

Primary osteoblast culture were prepared from 1-month-old WT/Vps35$^{+/-}$ or 3-month-old OcnCre/Vps35Ocn-CKO mice long bones. Briefly, small bone pieces were incubated in collagenase solution to remove all remaining soft tissue and adhering cells, then transfer to 60 mm culture dishes containing DMEM medium supplemented with 10% FBS, 1% penicillin/streptomycin, 10 mM β-glycerophosphate and 50 μM L-ascorbic acid-2-phosphate. Replace culture medium three times per week. Bone cells will start to migrate from the bone chips after 3–5 day. After two weeks, the monolayer is trypsinized by incubating the cells with trypsin solution. Cells were cultured in 60 mm dishes with α-MEM mineralizing medium containing 10% FBS, 1% penicillin/streptomycin, 2.5 mM β-glycerophosphate and 10^{-8} M Vitamin D3 for 2 days prior to co-culture with osteoclast precursors.

To isolate osteoclast precursors, total bone marrow is flushed from the long bones (femur and tibia) of 3-month-old WT mice with ice-cold α-MEM and plated on 100 mm culture dishes in α-MEM containing 10% FBS and 10 ng/ml recombinant M-CSF. Cells were incubated at 37 °C with 5% CO$_2$ overnight. Nonadherent cells were harvested and subjected to Ficoll-Hypaque gradient centrifugation for purification of BMMs. Cells were placed onto pre-sterilized glass coverslips in the 12-well plates in α-MEM containing 10% FBS and 10 ng/ml recombinant M-CSF. After a few days, the coverslips containing osteoclastic cells were seeded onto mineral thin films above WT or Vps35-KD osteoblasts already plated on the 100 mm culture dishes. For the sham control group, cells were cultured in α-MEM medium supplemented with 10% FBS, 1% penicillin/streptomycin and 2.5 mM β-glycerophosphate. Other groups were treated with PTH$_{(1-34)}$ intermittently (iPTH) (100 nM, 1-h per day) or continually (cPTH)(100 nM), or Vitmin D3(10^{-8} M, daily change with fresh medium). The co-cultures were grown for 10–12 days and prepared for TRAP staining.

2.6. Immunofluorescence Staining and Confocal Imaging Analysis

MC3T3-E1 cells plated onto coverslips were fixed with 4% paraformaldehyde at room temperature for 20 min, permeabilized in 0.15% Triton X-100 for 8 min, and then subjected to co-immunostaining analysis using indicated antibodies. The stained cells were washed 3 times with PBS and mounted with VECTASHIELD (H-1200; Vector Laboratories) for imaging analysis by Zeiss LSM 510 Upright Confocal Microscope with 405, 488, 561 and 633 lasers (Carl Zeiss; LSM 510 software) at room temperature. A Plan-Apochromat 63X/ 1.40 oil DIC M27 objective lens (Carl Zeiss) was used with Immersol 518 N (Carl Zeiss). The acquired 8-bit RGB images were exported to TIFF files with the LSM510 viewer software (Carl Zeiss). Photoshop software CS5 (Adobe) was used to adjust the brightness. Figures were constructed in Illustrator version CS5 (Adobe).

For fluorescent quantification, morphometric measurements of images were performed using NIH ImageJ and ZEN (Carl Zeiss) software. Two channels (red and green) were selected for colocalization analysis. Single labeled control samples (red or green) were prepared to accurately set the crosshairs. The controls were imaged with the same microscope setting as the double or triple labeled experimental samples. The pixel distribution of a red-only or a green-only population was examined, and the horizontal or vertical crosshair was set just above this population (The threshold was between 40–60, based on different experiments). The quadrants represent pixels that have high green and low red intensities, or high red and low green intensities were consider false colored. The quadrant represents pixels with high intensity levels in both green and red are considered to be co-localized.

2.7. Protein Extraction and Western Blot Analysis

For cell signaling experiments, MC3T3 or BMSCs were serum starved overnight and stimulated with PTH$_{(1-34)}$ (100 nM) or epinephrine (300 nM) for indicated time in the figure legend, and the total protein was extracted with lyses buffer, which contained 50 mM Tris-HCl (pH 7.5), 150 mM NaCl, 1%(v/v) Triton X-100, 0.1% SDS, 0.5% deoxycholate and 1 mM EDTA, supplemented with protease inhibitors (1 μg/ml leupeptin and pepstatin, 2 μg/ml aprotinin and 1 mM PMSF) and phosphatase inhibitors (10 mM NaF and 1 mM Na$_3$VO$_4$). The protein was propelled by western blot analyses.

2.8. Measurement of cAMP Production

Levels of cAMP were measured using a commercially available cAMP complete ELISA kit (Enzo Life Sciences, Farmingdale, NY, USA). MC3T3 cells or BMSCs were plated in 12-well plates with the same cell density. Cells were serum starved overnight and stimulated with PTH$_{(1-34)}$ (100 nM) or Forskolin (10 μM) for the indicated time. Then, cells were lysed for 10 min with 0.1 M HCl, centrifuged at 600 g at room temperature. The supernatant were assayed as described by the manufacturer.

2.9. Micro-computed Tomography (μCT)

The μCT analyses were carried out as described previously (Xia et al., 2013a; Xia et al., 2013b). In brief, micro-architecture of the distal trabecular bone and mid-shaft cortical bone of the femurs from 3-month or older mice were measured by Scanco μCT 40 (Scanco Medical AG, Brüttisellen, Switzerland).

The scan of the trabecular bone was performed from the growth plate, and consisted of 200 slices (each slice was 12 μm in thickness). The 3-D reconstruction was performed using all the outlined slices. No cortical bone was included in this analysis. Data was obtained on bone volume (BV), total volume (TV), BV/TV, bone density, trabecular number and connectivity.

The scan of the cortical bone was performed at the mid-shaft of the femur and consisted of 25 slices (each slice was 12 μm in thickness). There was no trabecular bone in these images at the mid-shaft. Cortical bone was thresholded at 329, and the 3-D reconstruction was performed on all 25 slices. Data was obtained on BV, TV, BV/TV, bone density, and cortical thickness.

2.10. Bone Histomorphometric Analysis

Bone histomorphometric analyses were carried out as previously described (Cui et al., 2010; Xia et al., 2013a; Xia et al., 2013b; Zhou et al., 2008; Zhou et al., 2006). In brief, mouse tibia and femurs were fixed overnight in 10% buffered formalin, decalcified in 14% EDTA, embedded in paraffin, sectioned, and subjected for H & E and TRAP staining analyses, which were counter stained by fast green. Bone histomorphometric perimeters were determined by measuring the areas situated at least 0.5 mm from the growth plate, excluding the primary spongiosa and trabeculae connected to the cortical bone.

2.11. Measurements of Serum Levels of Osteocalcin, PYD, and Calcium

Mouse serum samples were collected and allowed to clot for 30 min and then centrifuged for 10 min at 3000 rpm. Serum was frozen at −80 °C until use. Mouse osteocalcin Elisa kit (Biomedical Technologies, Inc.), METRA Serum PYD RIA kit (QUIDEL Corporation), and Calcium Detection Kit (Abcam) were used to measure mouse serum levels of osteocalcin, PYD and calcium as described previously (Cui et al., 2010; Xia et al., 2013b; Zhou et al., 2006). All the assays were carried out per the instructions. All the samples were measured in duplicate, the ODs measured after reactions were converted to osteocalcin/PYD/calcium concentration using their standard curves, and values were subjected to statistical analysis.

2.12. RNA Isolation and Real Time-PCR

Primary cultured BMSCs or MC3T3 were treated without PTH (Sham control) and with PTH$_{(1-34)}$ intermittently (iPTH) (100 nM, 1-h per day, for 6 days) or continually (cPTH)(100 nM, daily change with fresh medium containing PTH$_{(1-34)}$). For short time course to confirm the transcript stability of RANKL or OPG (Fu et al., 2002), BMSCs or MC3T3 were treat with PTH$_{(1-34)}$ (100 nM) for 0, 1, 2, 4, 6 and 12 h. Total RNA was isolated from BMSCs or MC3T3 by Trizol extraction (Invitrogen, Carlsbad, CA, USA). Q-PCR was performed with a Quantitect SYBR Green PCR Kit (Bio–Rad), according to the manufacturers's instruction, and with a Real-Time PCR System with analytical software (Opticon Monitor 3). The following primers were used: Osteocalcin, 5′-CTGGCTGCGCTCTGTCTCT-3′ and 5′-TGCTTGGACATGAAGGCTTTG-3′; RANKL, 5′-ATCCCATCGGGTTCCCATAA-3′ and 5′-TCCGTTGCTTAACGTCATGTTAG-3′; OPG, 5′-GGCCTGATGTATGCCCTCAA-3′ and 5′-GTGCAGGAACCTCATGGTCTTC-3′; MEPE, 5′-GCAGGTGGGAGCCTTGTG-3′ and 5′-GGCTGCCGGCATTAATTCT-3′. β-actin primers (5′-AGGTCATCACTATTGGCAACGA-3′ and 5′-CATGGATGCCACAGGATTCC-3′) were used for normalization.

2.13. Co-immunoprecipitation (Co-IP)

HEK293T cells were maintained in Dulbelcco's modified Eagle's medium supplemented with 10% (vol/vol) fetal bovine serum (Invitrogen). Transient transfection was performed with PEI. Transfected cells were harvested after 48 h in the following buffer: 50 mM Tris-HCl(pH 7.5); 150 mM sodium chloride; 1% Nonidet P40; 0.5% sodium deoxycholate, with protein inhibitor cocktail (Roche). Immunoprecipitation was performed with a 1/100 dilution of a rabbit polyclonal mCherry antibody or a mouse monoclonal V5 antibody against PTH1R-mCherry or PPP1R14C-V5. Western blotting was performed using the ECL procedure according to the manufacturer's instructions (Bio–Rad), with a mouse monoclonal Flag antibody to detect the co-immunoprecipitation Flag-Vps35 or anti-mCherry rabbit polyclonal antibody for PTH1R-mCherry proteins.

2.14. GST Pull-down Assays

GST and GST-PPP1R14C fusion proteins were expressed in IPTG-stimulated (1 mM final concentration) BL21 Escherichia coli. Bacterial cell lysates were allowed to bind to the glutathione-Sepharose 4B beads (GE Health Sciences). Flag-Vps35 and PTH1R-mCherry proteins were synthesized in HEK293 cells. The GST pull-down assays was performed by incubation GST beads with each extract for 1 h at 4 with constant mixing. After washing GST beads five times with PBS and eluting proteins with SDS sample buffer, western blots were performed.

2.15. Statistical Analysis

All data were expressed as mean ± SD. For in vivo studies, 5–6 mice per genotype per assay were used. For in vitro cell biological and biochemical studies, each experiment was repeated 3 times. 10–50 cells were quantified for immunostaining analyses. The significance level was set at $P < 0.05$, the Student t-test, two-way ANOVA and post-hoc test (GraphPad Prism 5) were used.

3. Results

3.1. PTH$_{(1-34)}$ Stimulation of PTH1R-VPS35 Interaction and Their Translocation to the Golgi in MC3T3 Cells

In light of the observations that VPS35 regulates PTH1R's trafficking and signaling in HEK293 cells (Feinstein et al., 2011), and both VPS35 and PTH1R are highly expressed in OBs (Simmonds and Kovacs, 2010; Vilardaga et al., 2012; Xia et al., 2013b), we speculate a crucial role for VPS35 to play in regulating PTH1R's trafficking, signaling, and function in OB-lineage cells. To test this speculation, we first examined exogenous PTH1R's trafficking in control and Vps35-deficient MC3T3 cells, an osteoblastic cell line that responses to PTH$_{(1-34)}$ stimulation (Issack et al., 2007; Moriya et al., 2015; Schiller et al., 1999). A plasmid encoding PTH1R-mCherry fusion protein was generated, which is a similar fusion protein as PTH1R-EGFP that is often used in the literature to image PTH1R's distribution (Feinstein et al., 2011) (Fig. S1A). When expressed in MC3T3 cells, the PTH1R-mCherry displayed a cell surface and vesicle-like punctae distribution pattern, which could be recognized by anti-PTH1R (Fig. S1B). Upon PTH$_{(1-34)}$ stimulation, the PTH1R-mCherry expressing cells, but not controls, exhibited an increase in cAMP (Fig. S1C) and phospho-CREB (Fig. S1D–S1E), demonstrating the sufficiency and specificity of PTH1R-mCherry in mediating PTH signaling. We then used this fusion protein to examine its co-localizaion with endogenous VPS35 in MC3T3 cells. Very few punctae with PTH1R-VPS35 co-localization was detected in the basal culture condition (Fig. 1A). However, upon PTH$_{(1-34)}$ stimulation, their co-localization was increased in a time-dependent manner: peaked at 30 min, but declined at ~45 min of stimulation (Fig. 1A–B). The increase in PTH1R-VPS35 complex formation by PTH$_{(1-34)}$ was verified by co-immunoprecipitation analysis (Fig. 1C, D). It is noteworthy that the PTH1R-VPS35 complex was translocated to perinuclear organelles in response to PTH$_{(1-34)}$ stimulation (Fig. 1A, E), which we determined to be the Golgi apparatus by co-localization with the Golgi marker GM130 (Fig. 2A). The time course of PTH$_{(1-34)}$-induced PTH1R-VPS35 co-localization correlated well with that of PTH1R-VPS35 translocation to the Golgi (Fig. 1A–B, E), but slower to decline, as compared with the time course of cAMP signaling (Fig. 1B). These results demonstrate a time-dependent increase of PTH1R interaction with VPS35 as well as PTH1R translocation to the Golgi by PTH$_{(1-34)}$, in line with the view for PTH1R as a cargo of
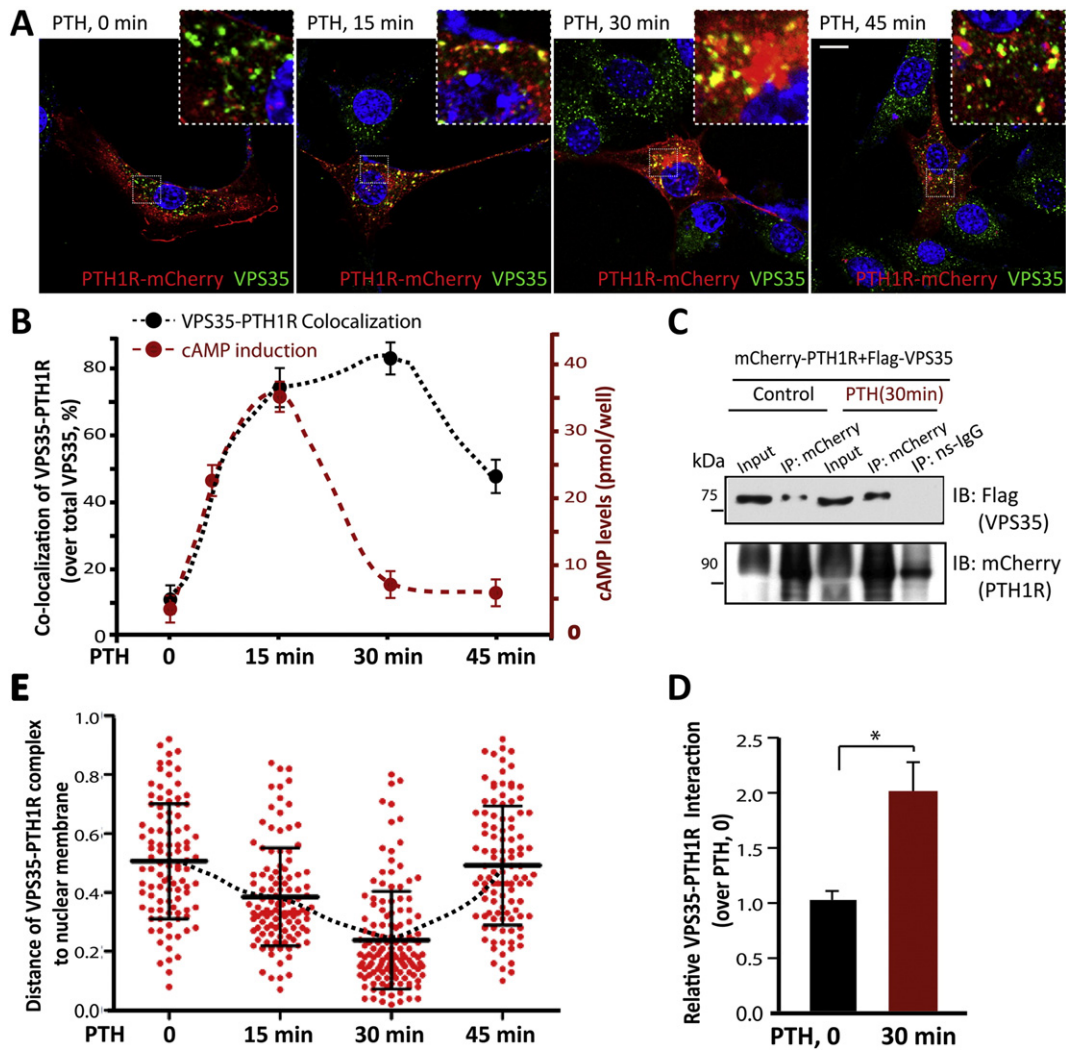
Fig. 1. PTH$_{(1-34)}$-increase of PTH1R interaction with VPS35 and PTH1R translocation to the TGN. (A–B) VPS35-PTH1R co-localization in MC3T3 cells was increased by PTH$_{(1-34)}$ stimulation. MC3T3 cells were transfected with PTH1R-mCherry, and then stimulated with PTH$_{(1-34)}$(100 nM) for 0, 15 min, 30 min and 45 min. Cells were fixed and immunostained with indicated antibodies. (A) Representative images. Images marked with white squares were amplified and shown in right top images. Bar, 10 μm. (B) Quantification analysis of data from A using ZEN and ImageJ as described in Materials and Methods. The co-localization index of PTH1R-mCherry with VPS35 was determined by the measurement of overlapped signal (yellow fluorescence) over total VPS35 signal. The means ± SEM ($n = 20$ cells from 3-different assays) were presented. *, $P < 0.05$. (C–D) VPS35-PTH1R co-immunoprecipitation was increased by PTH$_{(1-34)}$. HEK293T cells were transfected with indicated plasmids. 48-h post transfection, cell lysates (~500 μg) were immunoprecipitated by *anti*-mCherry antibody (for PTH1R) and anti-non-specific IgGs (a non-specific control). The resulting lysates were subjected to Western blot analysis using indicated antibodies. ~50 μg of cell lysates were used as inputs. Note that a weak mCherry signal was detected in the non-specific IgG immunoprecipitates in 1C, which might be due to a non-specific association of mCherry proteins with the IgG. The data presented is a representative of 3-independent experiments. The data were quantified and shown in right as means ± SEM. *, $P < 0.05$. (E) The distance ($\times 10$ μm) of Vps35-PTH1R co-distribution puncta to the nuclear membrane were presented.

VPS35/retromer not only in HEK293 cells (Feinstein et al., 2011), but also in the osteoblastic cell line.

3.2. Reduced PTH$_{(1-34)}$-driven PTH1R Translocation to the Golgi, But Increased PTH$_{(1-34)}$-driven Signaling, in Vps35-deficient MC3T3 and Primary OB-lineage Cells

We next examined VPS35's function in PTH$_{(1-34)}$-induced PTH1R translocation to the Golgi. This event required VPS35 expression in MC3T3 cells, as PTH$_{(1-34)}$-induced PTH1R translocation to Golgi was detected in control cells, but reduced in Vps35-KD (knock-down by miRNA-Vps35) MC3T3 cells (Fig. 2A–B). We then tested if PTH1R distribution in endosomes was increased in Vps35-KD cells, as most retromer cargos do. PTH1R in EEA1$^+$ early endosomes was unchanged in response to PTH$_{(1-34)}$ stimulation or Vps35-deficiency (Fig. 2C–D). However, PTH1R in LAMP1$^+$ late endosomes/early lysosomes was

increased in PTH$_{(1-34)}$-stimulated Vps35-KD MC3T3 cells (Fig. 2E–F). In line with this observation, PTH1R-mCherry was less stable when Vps35 was suppressed, with a shorter half-live (~4 h) in Vps35-deficient HEK293 cells than that of control cells (~8 h of half live)(Fig. S2). These results thus demonstrated the necessity of VPS35 in retrieval of PTH1R from late endosomes/lysosomes to the Golgi and thus preventing PTH1R degradation.

To investigate functional significance of VPS35-regulation of PTH$_{(1-34)}$-induced PTH1R translocation, we examined PTH$_{(1-34)}$-driven signaling dynamics in control and Vps35-KD MC3T3 cells (by infecting lentivirus encoding shRNA-Vps35). MC3T3 cells infected with lentiviruses of shRNA-Vps35 exhibited ~80% reduction of endogenous Vps35's expression (Fig. 3C). PTH$_{(1-34)}$-induced signaling events include cell surface (such as Gαs-mediated cAMP induction) and endosomal (such as phosphorylations of Erk1/2 and Akt) pathways, and both are important for PTH functions (Vilardaga et al., 2012). As shown in Fig. 3A, the cAMP
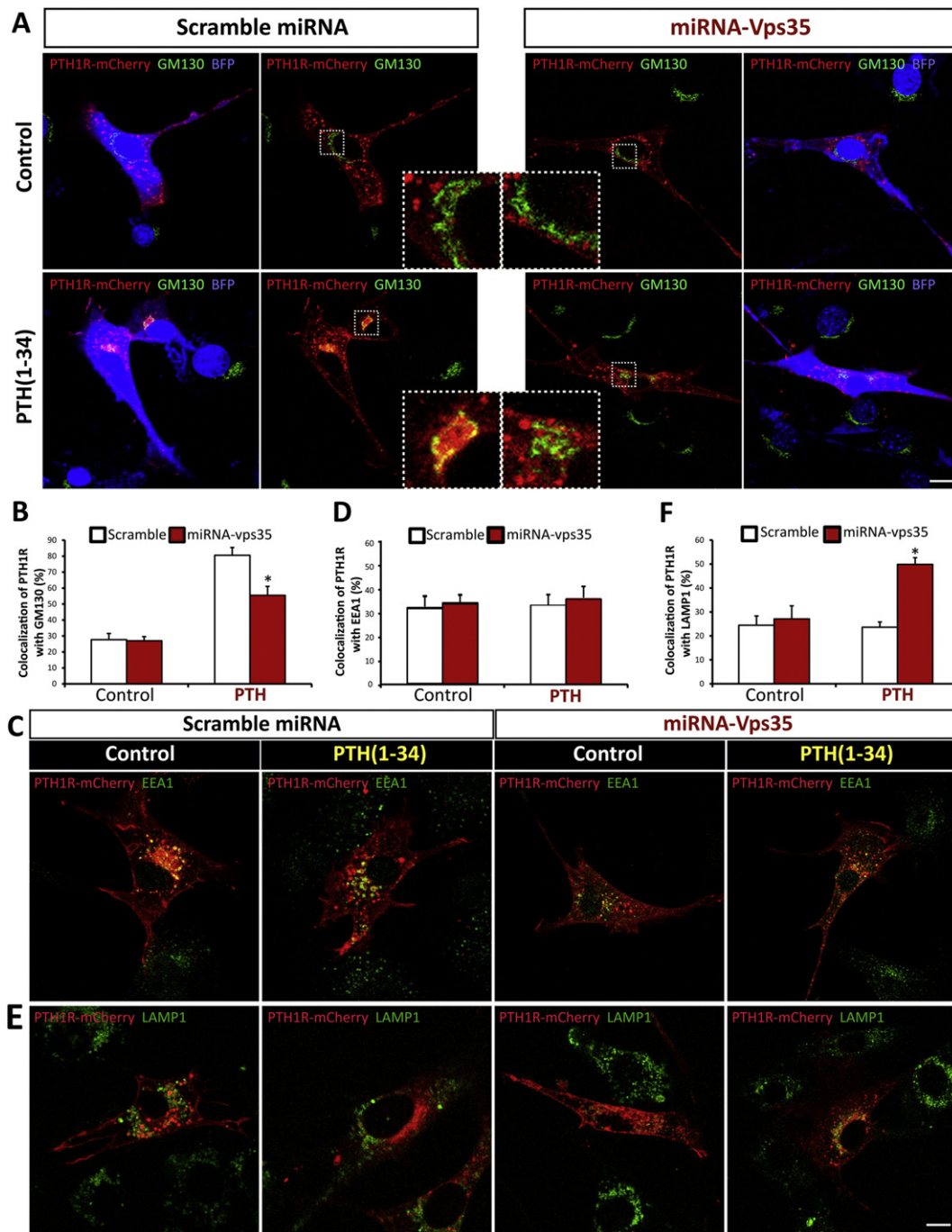
Fig. 2. Impaired PTH1R trafficking to TGN in VPS35-deficient MC3T3 cells. Co-immunostaining analysis of PTH1R-mCherry with GM130 (a marker for Golgi), EEA1 (a marker for early endosomes) or Lamp1 (a marker for late endosomes and early lysosomes) in control and Vps35-KD (by its miRNA) MC3T3 cells that were treated with or without $PTH_{(1-34)}$ (100 nM, 30 min). (A, C, and E) Representative images. Images marked with white squares in (A) were amplified and shown in middle images. Bar, 10 μm. (B, D, and F) Quantification analysis of data from A, C and E using ZEN and ImageJ as described in Materials and Methods. The co-localization index of PTH1R-mCherry with indicated markers (GM130, EEA1 and LAMP1) was determined by the measurement of overlapped signaling (yellow fluorescence) over total PTH1R-mCherry signal. The values of means ± SD ($n = 20$ cells from 3-different assays) were show. *, $P < 0.05$.

levels in control MC3T3 cells were induced by $PTH_{(1-34)}$ in a time dependent manner: increased at 5-min, peaked at 15-min, and declined at 30 min after $PTH_{(1-34)}$ stimulation. In Vps35-KD MC3T3 cells, the cAMP levels were further increased, and the time course was sustained in response to $PTH_{(1-34)}$, compared with that of control MC3T3 cells (Fig. 3A). This effect was specific, as the cAMP levels induced by forskolin, an activator of adenylate cyclase (AC), were slightly lower in Vps35-KD MC3T3 cells than that of controls (Fig. 3B). These results thus demonstrate a specific inhibitory role of VPS35 in $PTH_{(1-34)}$-induced cAMP/cell surface signaling.

We then examined $PTH_{(1-34)}$-induced phosphorylations of Erk1/2 (pErk1/2) and Akt (pAkt), in addition to pCREB (a downstream of cAMP-PKA pathway). Interestingly, they were all increased, and their time courses were also sustained in $PTH_{(1-34)}$-stimulated Vps35-KD MC3T3 cells, as compared with that of controls (Fig. 3C–D). The total protein levels of Erk1/2, Akt, and CREB were unchanged in Vps35-KD cells (Fig. 3C). However, the basal levels of pCREB, pErk1/2, and pAkt in Vps35-KD MC3T3 cells appeared to be higher than those in control cells (Fig. 3C). After normalization with their basal levels, $PTH_{(1-34)}$-induced pCREB, pErk1/2, and pAkt remained to be sustained as compared
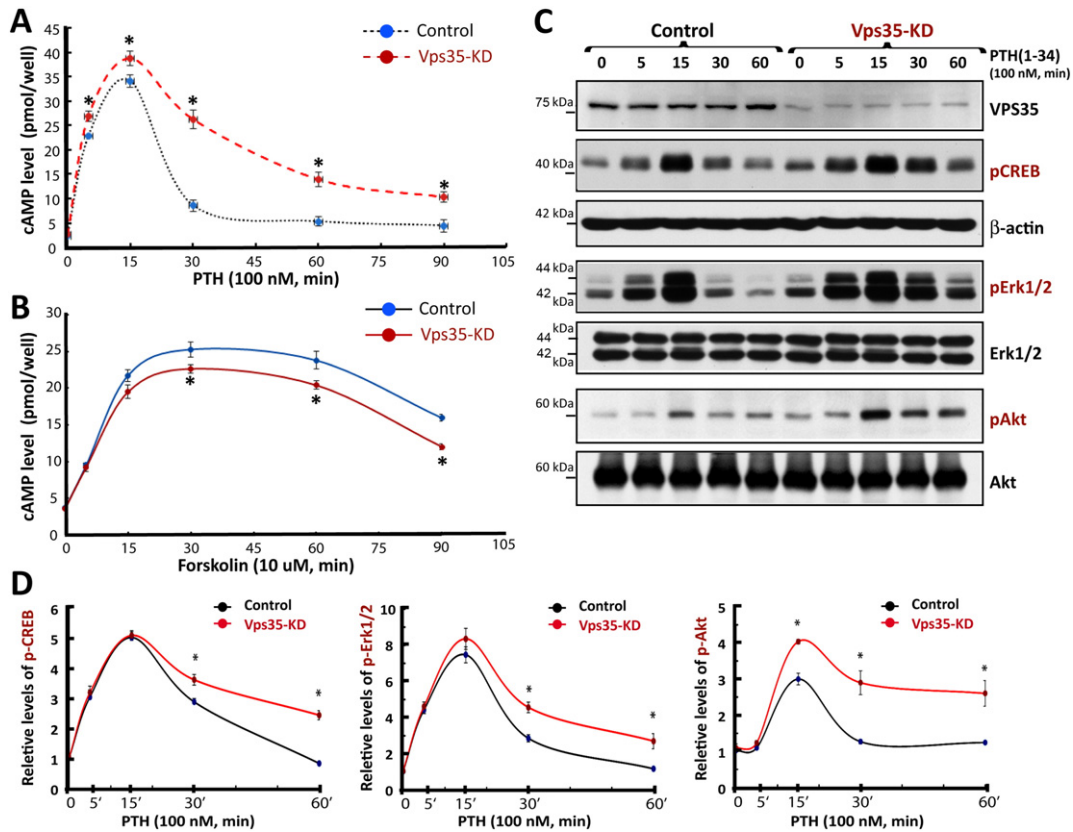
Fig. 3. Increased and sustained PTH$_{(1-34)}$-driven signaling in Vps35-deficient MC3T3 cells. Cells were serum starved overnight and stimulated with PTH$_{(1-34)}$ (100 nM) or Forskolin (10 μM) for the indicated time. For cAMP assay in (A–B), cells were lysed with 0.1 M HCl and centrifuged, the supernatant were assayed by using a cAMP ELISA kit. For Western blot analyses in (C–D), cell lysates were subjected to Western blot analyses using indicated antibodies. Representative blots were shown in C, and quantification analyses (by ImageJ software) of the data in C were shown in D. The values of mean ± SD from 3 separate experiments were shown. *, $P < 0.05$.

with that of controls (Fig. 3D). These results thus suggest that VPS35 in MC3T3 cells plays a negative role in regulating PTH$_{(1-34)}$-driven signaling, both cAMP induction and phosphorylations of CREB, Erk1/2, and Akt.

PTH$_{(1-34)}$-increase of pCREB in Vps35-KD MC3T3 cells was further confirmed by immunostaining analysis. The pCREB was mainly distributed in the nuclei, which was slightly increased by PTH$_{(1-34)}$ (Fig. S3A–B), but was obviously increased in the nuclei of Vps35-KD MC3T3 cells, compared with control MC3T3 cells after PTH$_{(1-34)}$ stimulation (Fig. S3A, S3C). This event was specific, as it was not increased in scramble RNAi expressing MC3T3 cells (Fig. S3A, S3C). Interestingly, a synergistical elevation in pCREB level was detected in Vps35-KD MC3T3 cells expressing PTH1R-mCherry, compared with the expression of PTH1R-mCherry or Vps35-KD alone (Fig. S3C). Taken together, these results indicate that VPS35 plays a critical role in deregulating PTH1R signaling, both cell surface and endosomal pathways, implicating VPS35 in PTH$_{(1-34)}$-induced functions.

3.3. Impairment in PTH$_{(1-34)}$-driven Catabolic Response, but Enhancement in PTH$_{(1-34)}$-induced Anabolic Response, in Vps35$^{+/-}$ BMSCs and Mice

We next investigated if VPS35 plays a role in regulating PTH$_{(1-34)}$-driven anabolic and/or catabolic responses. First, primary cultured BMSCs derived from Vps35$^{+/+}$ and $^{+/-}$ mice were treated with PTH$_{(1-34)}$ in two settings (Fig. 4A). One is intermittent treatment of PTH$_{(1-34)}$ (iPTH) (100 nM, 1 h/day, for 6 days), which induces anabolic response; and another one is continued treatment (cPTH)(100 nM, 24 h/day, for 6 days) that stimulates catabolic reaction (Fig. 4A) (Huang et al., 2004; Schiller et al., 1999). As shown in Fig. 4B, iPTH treatment resulted in a slight increase in expression of osteocalcin and RANKL in both Vps35$^{+/+}$ and $^{+/-}$ BMSC cultures, compared to sham

controls. No difference was detected between Vps35$^{+/+}$ and $^{+/-}$ cultures in responses to control or iPTH treatments (Fig. 4B–C), suggesting normal basal and anabolic-like responses in the mutant culture. In contrast, the catabolic response induced by cPTH treatment was different between Vps35$^{+/+}$ and $^{+/-}$ BMSC cultures (Fig. 4B–C). The cPTH treatment was capable to induce a catabolic-like response (e.g., decreased expression of osteocalcin and OPG, but increased RANKL-expression) in Vps35$^{+/+}$ cultures (Fig. 4B–C), but failed to do so in Vps35$^{+/-}$ cultures (Fig. 4B). The expression of OPG, osteocalcin, and MEPE (matrix extracellular phosphoglycoprotein), but not RANKL, was markedly elevated in Vps35$^{+/-}$ cultures with cPTH stimulation (Fig. 4B), resulting in a decreased ratio of RANKL over OPG in Vps35$^{+/-}$ BMSCs following cPTH-stimulation, as compared with that of Vps35$^{+/+}$ controls (Fig. 4C). Together, these results suggest that Vps35-deficiency in OB-lineage cells causes a weak increase in PTH$_{(1-34)}$-driven anabolic response, but a major decrease in PTH$_{(1-34)}$-induced catabolic response.

Second, we examined VPS35's function in PTH$_{(1-34)}$-induced catabolic response by an in vitro osteoclastogenesis co-culture assay. In this assay, wt-BMMs were co-cultured with wt-OBs or Vps35$^{+/-}$ OBs in the absence of exogenous RANKL, but presence of control (PBS), iPTH, or cPTH stimulations. At day 7 of the co-culture, cells were stained with TRAP, and TRAP$^+$ MNCs (multi-nuclei cells)(an indicator for osteoclastogenesis) were quantified. As shown in Fig. 4D–E, iPTH treatments induced comparable numbers of TRAP$^+$ MNCs between wt- and Vps35-deficient OB co-cultures. However, cPTH treatments resulted in a significant less TRAP$^+$ MNCs formed in Vps35-deficient OBs than those in wt-OBs co-cultures (Fig. 4D–E). These results thus provide additional evidence for an impaired cPTH-driven catabolic response in Vps35$^{+/-}$ OB-lineage cells.

Third, we tested PTH$_{(1-34)}$'s function in Vps35$^{+/+}$ and $^{+/-}$ mice. PTH$_{(1-34)}$ was applied to Vps35$^{+/+}$ and $^{+/-}$ mice at age of P50 (sc,

50 μg/kg, 5 times/wk) for 5 weeks (Fig. S4A). At age of P85, mice were sacrificed, and their femur bone and serum samples were collected and subjected for further analyses (Fig. S4A). Measuring serum levels of pyridinoline (PYD)(a marker for bone resorption or catabolic response of PTH) showed an increase in Vps35$^{+/+}$, but not in Vps35$^{+/-}$, mice in response to PTH$_{(1-34)}$ treatment, compared with that of vehicle controls (Fig. S4I), supporting the view for an impairment in PTH$_{(1-34)}$-induced catabolic response in Vps35$^{+/-}$ mice. In contrast, a more

dramatic increase in serum osteocalcin levels (a bone formation marker) was also detected in PTH$_{(1-34)}$-injected Vps35$^{+/-}$ mice than that in Vps35$^{+/+}$ controls (Fig. S4J), in line with the notion for an increased anabolic response. In agreement with these views were observations from microCT (μCT) analysis, which showed a more dramatic increase in trabecular bone volumes in PTH$_{(1-34)}$-injected Vps35$^{+/-}$ mice than that in Vps35$^{+/+}$ littermate controls (Fig. S4B–S4H). The osteoporotic deficit in young adult Vps35$^{+/-}$ mice was diminished by PTH$_{(1-34)}$
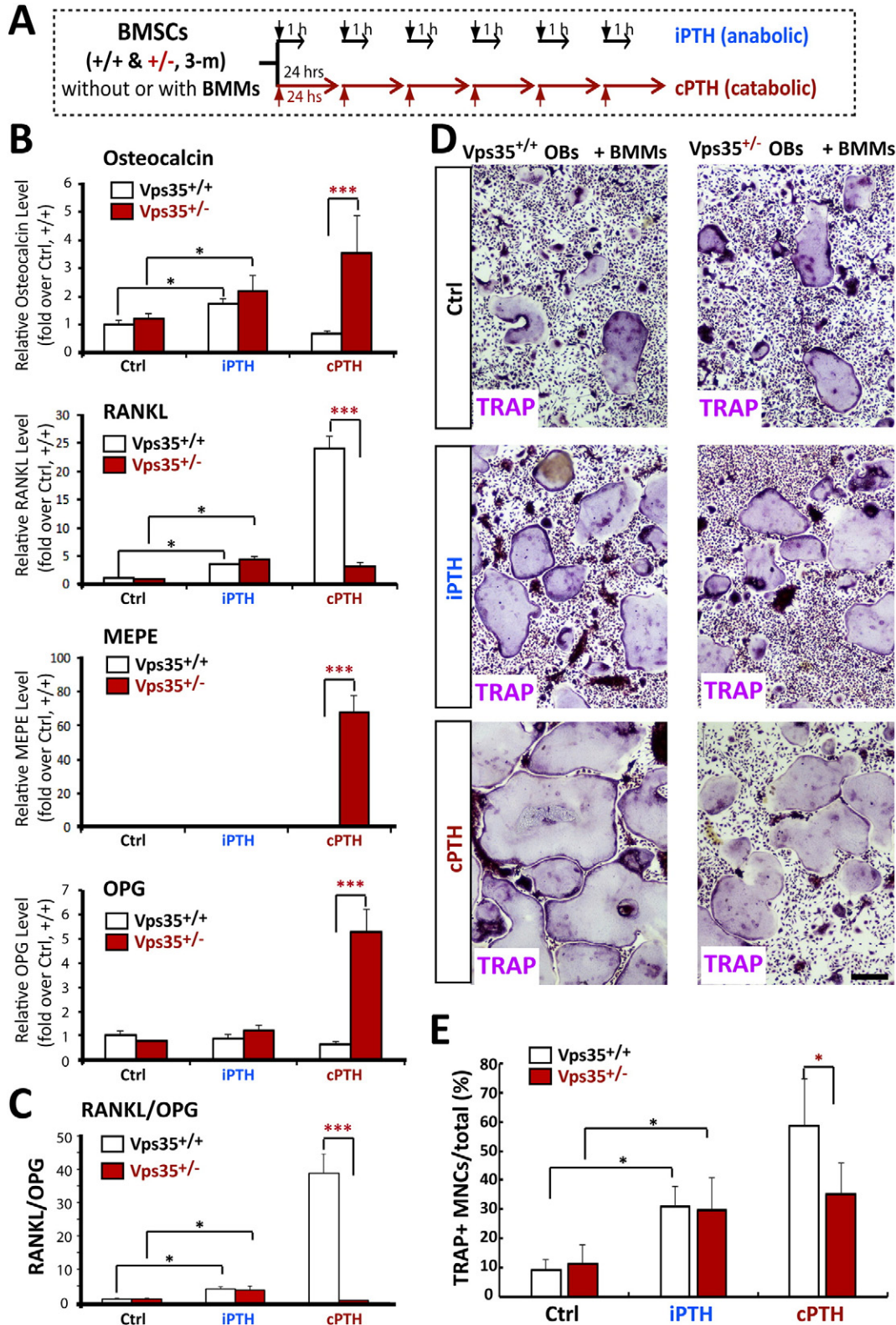
treatment (Fig. S4B–S4E). Further analysis of the trabecular thickness (TB. Th.), numbers (TB. N.), and connectivity (CD) revealed that PTH$_{(1-34)}$ increased TB.Th. in both Vps35$^{+/+}$ and $^{+/-}$ mice (Fig. S4F), but reduced TB.N. and CD only in Vps35$^{+/+}$, but not $^{+/-}$ mice (Fig. S4G–S4H). Taken together, Vps35$^{+/-}$ mice showed more dramatic PTH$_{(1-34)}$-induced anabolic response, but an impaired catabolic response, demonstrating a necessity of VPS35 for PTH$_{(1-34)}$-induced catabolic response in vivo.

3.4. Enhanced PTH$_{(1-34)}$-increased Anabolic Response With an Impaired Catabolic Response by Selective Deletion of VPS35 Gene in Mature OB-lineage Cells

VPS35 is expressed in both OB- and OC-lineage cells (Xia et al., 2013b). We thus asked whether VPS35 in OB-lineage cells is required for PTH$_{(1-34)}$-induced catabolic response in vivo. To this end, we generated OB-selective Vps35 knocking out mice, Vps35$^{Ocn-Cre}$, by crossing the floxed allele (Vps35$^{f/f}$) with the osteocalcin (Ocn)-Cre. VPS35 protein was selectively reduced in OB-lineage cells, but not BMMs, derived from Vps35$^{Ocn-Cre}$ mice, compared with that of controls (Vps35$^{f/f}$ mice)(Fig. S5C). As Vps35$^{+/-}$ mice (Xia et al., 2013b), Vps35$^{Ocn-Cre}$ mice at young adult age (3-month old) had normal body weight (Fig. S5A–S5B), but displayed osteoporotic deficits, including decreased trabecular and cortical bone-mass and reduced serum osteocalcin level (Fig. 5, and S5D–S5F). PTH$_{(1-34)}$ was then applied to Vps35$^{Ocn-Cre}$ and control (Vps35$^{f/f}$) mice at age of P50 (sc, 50 μg/kg, 5 times/wk) for 5 weeks as described in Fig. S4A. After PTH$_{(1-34)}$ injections, Vps35$^{Ocn-Cre}$ mice showed more dramatic anabolic response, such as increases in trabecular bone volumes and trabecular thickness (TB. Th.), as well as the serum osteocalcin levels than those of control mice (Fig. 5A–F). The catabolic response, viewed by increased serum PYD and calcium levels, was detected in control, but not Vps35$^{Ocn-Cre}$ mice (Fig. 5G–H). The osteoporotic deficit in Vps35$^{Ocn-Cre}$ mice was also diminished by PTH$_{(1-34)}$ treatment (Fig. 5).

Moreover, as Vps35-KD MC3T3 cells, PTH$_{(1-34)}$-driven signalings, including cell surface signaling (cAMP induction) and endosomal signaling (pCREB, pErk1/2, and pAKT), were all increased, and their time courses were sustained in BMSCs from Vps35$^{Ocn-Cre}$ mice, compared with that of controls (Fig. 6A–C).

Furthermore, we examined osteocalcin, RANKL and OPG's expression in control (Vps35$^{f/f}$) and Vps35$^{Ocn-Cre}$ BMSCs in response to PTH$_{(1-34)}$ stimulation for a short time course (1, 2, 4, 6 to 12 h). As shown in Fig. 6D, osteocalcin's transcripts were slightly elevated in Vps35$^{Ocn-Cre}$ BMSCs, compared with those of controls, when PTH$_{(1-34)}$ was present for more than 6-h. PTH$_{(1-34)}$-induced RANKL's transcripts were comparable between control and Vps35$^{Ocn-Cre}$ BMSCs (Fig. 6E). However, OPG's transcripts were decreased in control cells, but increased in Vps35$^{Ocn-Cre}$ BMSCs, in response to PTH$_{(1-34)}$ stimulations (Fig. 6F). Thus, ratios of RANKL over OPG were much lower in PTH$_{(1-34)}$-stimulated Vps35$^{Ocn-Cre}$ BMSCs than those in control cells (Fig. 6G). These results support the view for an impaired PTH$_{(1-34)}$-driven catabolic response in Vps35–deficient OB-lineage cells.

Finally, we tested this view by examining osteoclastogenesis by the co-culture assay: wt-BMMs plus wt-OBs or Vps35$^{Ocn-Cre}$ OBs in the presence or absence of iPTH$_{(1-34)}$ or cPTH$_{(1-34)}$ or vitamin D3 stimulations.

The iPTH$_{(1-34)}$ or vitamin D3 treatments induced comparable numbers of TRAP$^+$ MNCs between wt- and Vps35$^{Ocn-Cre}$ OB co-cultures (Fig. 6H–I). Again, cPTH$_{(1-34)}$-induced TRAP$^+$ MNCs were much less in Vps35$^{Ocn-cre}$ OBs than those in wt-OBs co-cultures (Fig. 6H–I).

In aggregates, these results reconfirmed the necessity of VPS35 in OB-lineage cells to maintain bone-mass, to deregulate PTH$_{(1-34)}$-induced cell surface and endosomal signaling, to promote PTH$_{(1-34)}$-driven catabolic response, and thus to prevent a large bone-gain by PTH$_{(1-34)}$.

3.5. VPS35 Interaction With PPP1R14C, an Inhibitory Subunit of PP1 Phosphatase

To understand how VPS35 terminates PTH1R-mediated signaling, we searched for additional VPS35/retromer binding partners. PPP1R14C is one of the new VPS35/retromer binding partners identified by subcellular fractionation of retromer complex in Hela cells and proteomic analysis (Fig. 7A) (http://human.med.utoronto.ca/index.php). As PPP1R14C is an inhibitory subunit of PP1 serine/threonine phosphatase (Drgonova et al., 2010; Eto, 2009; Liu et al., 2002; Wenzel et al., 2007), we speculate that VPS35 may deregulate PTH1R signaling via its interaction with PPP1R14C. To test this view, we first verified VPS35's interaction with PPP1R14C in MC3T3 cells by co-immunostaining analysis. The endogenous PPP1R14C (revealed by the polyclonal anti-PPP1R14C antibody) was indeed co-localized with the exogenous GFP-VPS35 (Fig. 7B). Their co-localization appeared to be specific, as it was not detected between GFP-VPS35 with endogenous PPP1R14A, a PPP1R14C-family PP1 inhibitor (Fig. 7B–C). The anti-PPP1R14C antibody was also specific, as its immunostaining signal was abolished in cells knocking down of PPP1R14C (PPP1R14C-KD) (Fig. S6). We next confirmed VPS35 interaction with PPP1R14C by co-immunoprecipitation analysis (Fig. 7D–E). VPS35 was indeed detected in PPP1R14C-immunocomplex (Fig. 7D). The VPS35-PPP1R14C interaction was also enhanced by PTH$_{(1-34)}$ stimulation (Fig. 7D–I), but reduced by expression of PTH1R-mCherry (Fig. 7F–H). Moreover, we tested if VPS35 interaction with PPP1R14C is a direct binding. The recombinant GST-PPP1R14C fusion protein was generated and subjected to an in vitro GST pull down assay. Indeed, VPS35 was detectable in the precipitates pulled down by GST-PPP1R14C, but not GST (Fig. 7J), suggesting a direct interaction. Taken together, these results support the view for PPP1R14C as a VPS35/retromer binding partner in MC3T3 cells and implicate PPP1R14C's involvement in PTH signaling.

3.6. PPP1R14C Interaction With PTH1R, Which is Increased by PTH$_{(1-34)}$ Stimulation, but Suppressed by VPS35

Whereas PPP1R14C-VPS35 co-localization was reduced by PTH1R-mCherry, a co-localization of PPP1R14C with PTH1R-mCherry was noted (Fig. 7F–I). This co-localization was also increased by PTH$_{(1-34)}$ (Fig. 7G, I), implicating a possible interaction between PPP1R14C with PTH1R-mCherry. We thus carried out co-immunoprecipitation analysis to test this view. PTH1R was indeed detected in the immune-complex of PPP1R14C, so as VPS35 (Fig. 8A–C). The interaction was increased by PTH$_{(1-34)}$ stimulation (Fig. 8A–C). These results thus suggest that PTH$_{(1-34)}$ induced PTH1R interaction with VPS35, as well as PPP1R14C.

Fig. 4. Reduced PTH$_{(1-34)}$-driven catabolic response in Vps35-deficient BMSCs and mice. (A) Intermittent and continued treatments of PTH$_{(1-34)}$. Primary cultured BMSCs from Vps35$^{+/+}$ and Vps35$^{+/-}$ mice (at age of 3-month old) were treated without PTH (Sham control) and with PTH$_{(1-34)}$ intermittently (iPTH) (100 nM, 1-h per day, for 6 days) or continually (cPTH)(100 nM, daily change with fresh medium containing PTH$_{(1-34)}$). The total RNAs were isolated after treatments and subjected to real time PCR analysis. (B–C) Real-time PCR analysis of the mRNA levels of osteocalcin, MEPE, RANKL, and OPG. The values are normalized to β-actin. Ratio of RANKL/OPG was shown in C. The values of mean ± SD from 3-different experiments were presented. Data is determined by two-way ANOVA followed by a post-hoc text, *, $p < 0.05$, ***, $p < 0.001$, significant difference. (D–E) TRAP staining analysis of multiple nuclei cells (OCs) derived from BMMs co-culture with osteoblasts from Vps35$^{+/+}$ and Vps35$^{+/-}$ mice. The coverslips containing WT BMMs were seeded onto mineral thin films above Vps35$^{+/+}$ or Vps35$^{+/-}$ osteoblasts already plated on the 100 mm culture dishes. Cells were cultured in α-MEM medium supplemented with 10% FBS, 1% penicillin/streptomycin, 2.5 mM β-glycerophosphate and 10^{-8} M Vitamin D3 (first 2 days). Then, cells were treated with PBS (sham Control), PTH$_{(1-34)}$ intermittently (iPTH) (100 nM, 1-h per day) or continually (cPTH)(100 nM). The co-cultures were grown for 10 days and prepared for TRAP staining. Representative images are shown in D, the quantitative analyses of TRAP$^+$ multinuclei cells (MNCs) over total cells are presented in E. The values of mean ± SD from 3-different experiments were presented. Data is determined by two-way ANOVA *, $p < 0.05$, significant difference.
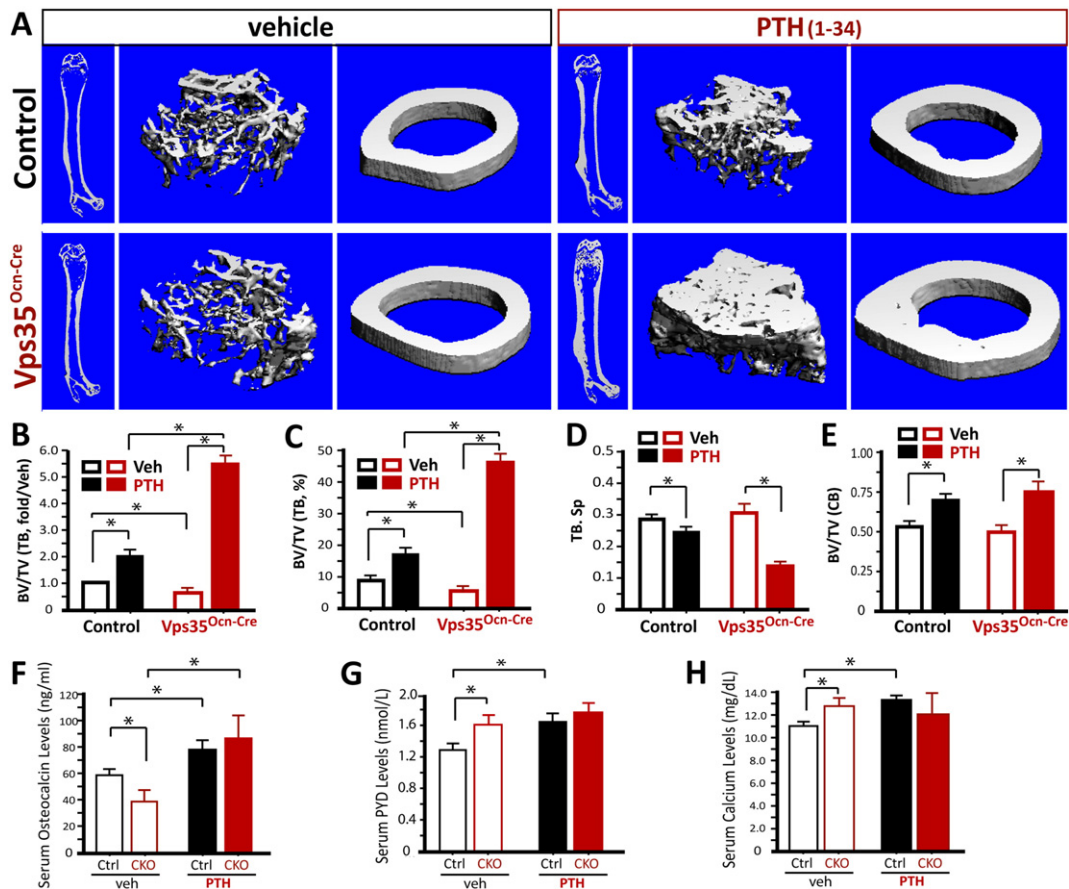
Fig. 5. Increased PTH$_{(1-34)}$-induced anabolic response, but impaired catabolic response, in Vps35$^{Ocn-Cre}$ mice. P50 old Vps35$^{f/f}$ and Vps35$^{Ocn-Cre}$ male mice were administered once daily injection of hPTH$_{(1-34)}$ (50 μg/Kg), or vehicle (0.9% sodium chloride), 5 days per week for 5 weeks. The femurs and sera samples collected after treatments were subjected to μCT and ELISA/RIA assays, respectively. (A–E) The μCT analysis of femurs from Vps35$^{f/f}$ and Vps35$^{Ocn-Cre}$ littermates (at age of P85) treated with vehicle or PTH$_{(1-34)}$. Five different male mice of each genotype per group were examined blindly. Representative 3D images were shown in A. Quantification analyses (mean ± SD, $n = 5$) were presented in B-D. Two-way ANOVA *, $P < 0.05$, **, $P < 0.01$, significant difference. (F–H) ELISA/RIA analysis of serum osteocalcin (F), PYD (G), and serum calcium (H) levels of Vps35$^{f/f}$ and Vps35$^{Ocn-Cre}$ littermates (at age of P85) treated with vehicle or PTH$_{(1-34)}$. Mean ± SD from 5 different animals per genotype. *, $P < 0.05$, significant difference.

As VPS35 interacts with both PTH1R and PPP1R14C, we wondered if PTH1R-PPP1R14C interaction was mediated or regulated by VPS35. To address this issue, we first asked if PTH1R interaction with PPP1R14C is a direct binding event. Again, the recombinant GST-PPP1R14C fusion protein was used for the in vitro GST pull down assay. As shown in Fig. 8D, PTH1R was present in the precipitates pulled down by GST-PPP1R14C, but not GST. This result supports the notion for a direct interaction between PTH1R and PPP1R14C, which is likely independent on VPS35. We second tested this view by carrying out PTH1R-PPP1R14C co-immunoprecipitation assays in Vps35-KD cells. Interestingly, suppressing VPS35's expression resulted in an even more PTH1R protein in PPP1R14C immune-complex upon PTH$_{(1-34)}$ stimulation, compared with that of VPS35-expressing cells (Fig. 8A–C), suggesting a negative regulation of PTH1R-PPP1R14C interaction by VPS35. Third, we tested this view by co-immunostaining analysis. The co-localization of PTH1R with PPP1R14C was induced in both control and VPS35-deficient MC3T3 cells by PTH$_{(1-34)}$ in a time-dependent manner (Fig. 8E–F). In control cells, their co-localization was peaked in 30 min, reduced in 45 min and after, of PTH$_{(1-34)}$ stimulation (Fig. 8E–F), corroborating well with that of PTH$_{(1-34)}$ signaling events. In Vps35-KD cells, more increase in PTH1R-PPP1R14C co-location was detected at 15- and 30-min of PTH$_{(1-34)}$ stimulation, compared with that of controls (Fig. 8E–F). Taken together, these results suggest that the two protein complexes, PTH1R-PPP1R14C and VPS35-PPP1R14C, in MC3T3 cells, are both increased by PTH$_{(1-34)}$ stimulation, but both complexes may suppress each other, implicating PPP1R14C in PTH signaling.

3.7. PPP1R14C's Contribution to the Enhanced PTH$_{(1-34)}$-driven Endosomal Signaling and Impaired Catabolic Response in Vps35-Deficient OB-lineage Cells

We then investigated PPP1R14C's role in regulating PTH$_{(1-34)}$ signaling and function. To this end, we generated shRNA-PPP1R14C plasmid and lentivirus, which efficiently suppressed exogenous and endogenous PPP1R14C expression (Fig. S6). MC3T3 cells were infected with lentiviruses encoding scramble shRNA (control), shRNA-PPP1R14C, shRNA-Vps35 (Vps35-KD), and shRNA-Vps35 plus shRNA-PPP1R14C (Vps35-KD + shR-PPP1R14C). In Vps35-KD MC3T3 cells, suppressing PPP1R14C by its shRNA abolished VPS35-deficiency enhanced and sustained PTH$_{(1-34)}$-driven pCREB, pErk1/2, and pAkt (Fig. 9A–B). In the presence of endogenous VPS35, suppression of PPP1R14C expression also reduced PTH$_{(1-34)}$-driven phosphorylations of CREB and Erk1/2 (Fig. S7). The increased PTH$_{(1-34)}$-driven pCREB in Vps35-KD cells was also attenuated by suppression of PPP1R14C by immunostaining analysis (Fig. 9C–D). These results suggest that PPP1R14C is not only required for efficient PTH signaling in WT cells, but also necessary for Vps35-deficiency-enhanced PTH$_{(1-34)}$ signaling, supporting the view for PPP1R14C as a positive regulator of PTH signaling. The latter view was further supported by the observations that expression of exogenous PPP1R14C enhanced PTH$_{(1-34)}$-driven pCREB signal in both control and Vps35-KD MC3T3 cells (Fig. S8).

We further asked if PPP1R14C is required for Vps35-deficiency enhanced PTH$_{(1-34)}$ induction of cAMP, a canonical pathway. To our
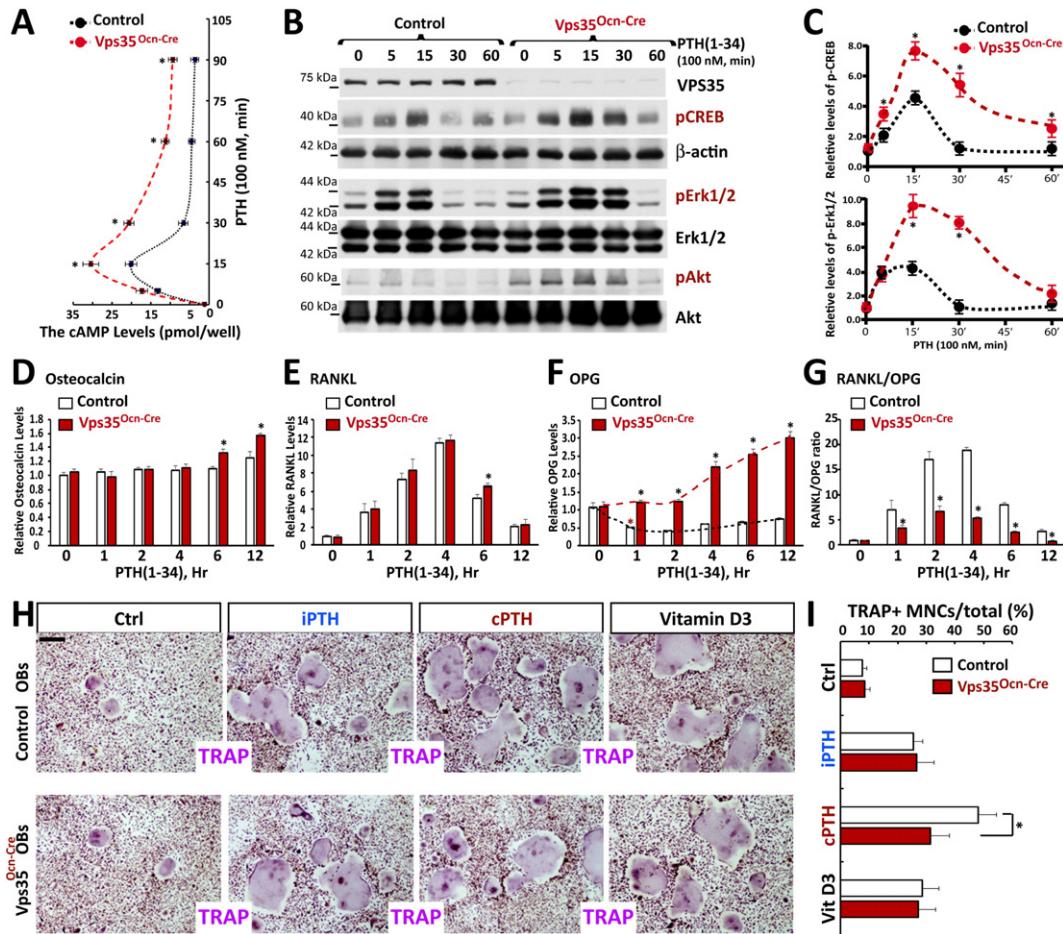
Fig. 6. Increased PTH$_{(1–34)}$-induced signaling and anabolic response, but reduced catabolic response, in BMSCs from Vps35$^{Ocn-Cre}$ mice. (A–C) Increased and sustained PTH$_{(1–34)}$-induced cAMP (A) and pCREB and pErk1/2 (B–C) in BMSCs from Vps35$^{Ocn-Cre}$ mice, compared with control BMSCs (from Vps35$^{f/f}$ mice). Cells were serum starved overnight and stimulated with PTH$_{(1–34)}$(100 nM) for the indicated time. For cAMP assay (in A), cells were lysed with 0.1 M HCl and centrifuged, the supernatant were assayed by using a cAMP ELISA kit. For evaluating protein phosphorylation assays (in B–C), cell lysates were subjected to Western blot analyses using indicated antibodies. Quantification analyses (in C) were carried out by ImageJ software) of the data in (B). The values of mean ± SD from 3 separate experiments were shown. *, $p < 0.05$. (D–G) Real-time PCR analysis of the mRNA levels of osteocalcin, RANKL, and OPG in BMSCs from control (Vps35$^{f/f}$) and Vps35$^{Ocn-Cre}$ mice. The values are normalized to β-actin. Ratio of RANKL/OPG was shown in G. The values of mean ± SD from 3-different experiments were presented. *, $P < 0.05$. (H–I) TRAP staining analyses of multiple nuclei cells (OCs) derived from co-cultures of BMMs plus osteoblasts (Vps35$^{f/f}$ vs Vps35$^{Ocn-Cre}$) in the presence of the indicated stimulations. Representative images were shown in (H), and quantification data (mean ± SD, $n = 3$ separate experiments) were presented in (I). *, $P < 0.05$.

surprise, little to no effect was detected in the cAMP induction by suppression of PPP1R14C in Vps35-KD cells, compared to Vps35-KD cells (Fig. 9E). In aggregate, these results support a working model, in which VPS35 deregulates both cell surface and endosomal PTH$_{(1–34)}$ signaling, but PPP1R14C appears to promote endosomal, but not cell surface cAMP, signaling (Fig. 9F).

We then addressed whether PPP1R14C is involved in the impaired PTH$_{(1–34)}$-driven catabolic response in Vps35-deficient cells. First, the control, Vps35-KD plus scramble shR, and Vps35-KD plus shR-PPP1R14C MC3T3 cells were treated with PTH$_{(1–34)}$ in two settings, iPTH and cPTH, as illustrated in Fig. 4A. As shown in Fig. 10A–10B, the iPTH treatment led to a significant increase in expressions of RANKL and OPG in control, Vps35-KD plus scramble shR, and Vps35-KD plus shR-PPP1R14C MC3T3 cells. The ratio of RANKL/OPG was not significantly altered among the three groups- control, Vps35-KD plus scramble shR, and Vps35-KD plus PPP1R14C-KD (Fig. 10C), supporting the view for a normal anabolic-like response in these cells. However, it is of interest to note that whereas Vps35-KD plus scramble shR MC3T3 cells showed an impairment in catabolic response induced by cPTH treatment (viewed by the ratio of RANKL/OPG)(Fig. 10C), such a catabolic response was nearly normal in cells of Vps35-KD plus shR-PPP1R14C (Fig. 10C). These results suggest an amelioration of the impaired catabolic response by suppressing PPP1R14C expression in

Vps35-deficient MC3T3 cells. We second tested this view by examining osteocalcin, RANKL and OPG's expression in these 3-groups of cells in response to PTH$_{(1–34)}$ stimulations for a short time course (1, 2, 4, 6 to 12 h). Note that PTH$_{(1–34)}$-induced RANKL's transcripts were comparable among the three-groups of MC3T3 cells (control, Vps35-KD plus scramble shR, and Vps35-KD plus shR-PPPP1R14C)(Fig. 10D). In contrast, OPG's transcripts were differentially regulated in the three-groups of cells by PTH$_{(1–34)}$: decreased in control cells, increased in Vps35-KD plus scramble shR cells, and without an change in Vps35-KD cells plus shR-PPP1R14C cells (Fig. 10E). Thus, suppression of PPP1R14C in Vps35-KD cells resulted in a partial restore of the catabolic response (e.g., ratio of RANKL/OPG) (Fig. 10F). In aggregate, these results demonstrate the necessity of PPP1R14C not only for the enhancement of the endosomal/non-canonical PTH$_{(1–34)}$ signaling, but also for the impairment in PTH$_{(1–34)}$-driven catabolic response due to Vps35-deficiency (Fig. 10G).

4. Discussion

There is increasing emphasis towards our understanding how PTH1R signaling is regulated, thus mediating PTH's dual functions: anabolic and catabolic responses. Here we provide several lines of evidence for VPS35, a major component of retromer, in regulating PTH1R
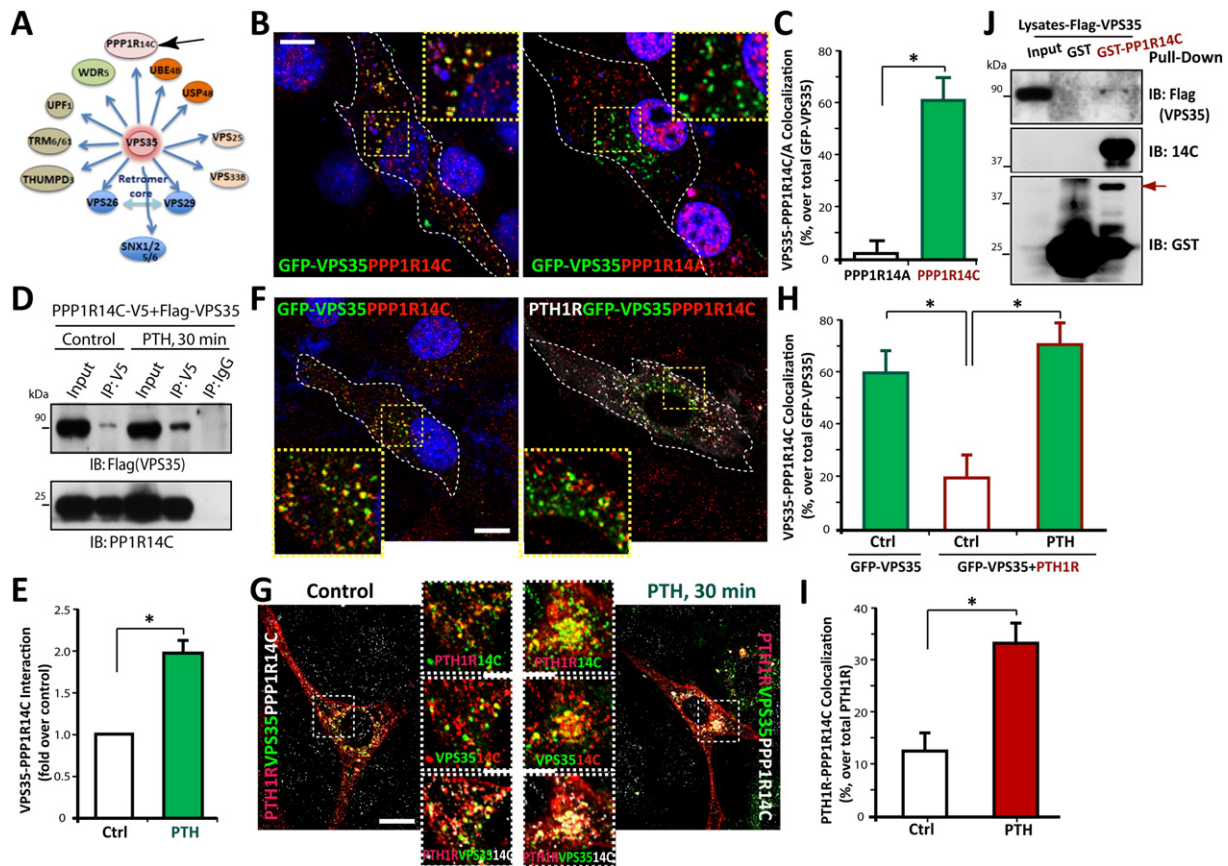
Fig. 7. VPS35 interaction with PPP1R14C. (A) Predicted proteins that may interact with VPS35 by Emililab. (B–C) Co-localization of endogenous PPP1R14C, but not PPP1R14A, with exogenous GFP-VPS35 in MC3T3 cells. Representative images were shown in (B). Quantification analyses of the optical intensity of GFP-Vps35 co-localization with PPP1R14A or PPP1R14C over total GFP-VPS35 were presented in C. Bar, 10 μm. (D–E) Co-immunoprecipitation of PPP1R14C with VPS35. HEK293T cells were transfected with V5-tagged PPP1R14C and FLAG-tagged VPS35. 48 h post transfection, cell extracts (~500 μg) were immunoprecipitated with V5(PPP1R14C), and the resulting immunoprecipitates were subjected to immunoblot using anti-Flag (for VPS35) antibody. IgG antibody was used as a negative control for immunoprecipitation, and 50 μg of the cell lysates was used as input. The data presented is a representative blot of 3 independent experiments. Quantification analyses were shown in E. (F–I) GFP-VPS35-PPP1R14C co-localization was decreased in MC3T3 cells expressing PTH1R-mCherry, but increased by PTH(1–34) stimulation. MC3T3 cells expressing PTH1R-mCherry and GFP-VPS35 were stimulated with control or PTH(1–34)(100 nM) for 30 min. Cells were fixed and subjected to the immunostaining analysis with indicated antibodies. Representative images were shown, and the images marked with white squares were amplified and shown in right corners. The quantification analyses of the optical intensity for the co-localization (GFP-VPS35 with endogenous PPP1R14C) over total GFP-VPS35 or the co-localization of PTH1R-PPP1R14C over total PTH1R were presented in H and I, respectively. Bar, 10 μm. The values of mean ± SD (n = 30 cells from 3-different experiments) were presented. *, P < 0.05. (J) In vitro GST pull down assay using indicated GST fusion proteins was carried out in HEK293 lysates expressing Flag-Vps35. The precipitates associated with the GST beads were subjected to the Western blot analysis using indicated antibodies.

trafficking, signaling, and function in OB-lineage cells in culture and in vivo. First, VPS35 promotes PTH(1–34)-induced PTH1R translocation to the Golgi apparatus, which appears to be critical not only for retrieval of PTH1R from lysosomes to prevent its degradation, but also for termination of PTH1R signaling. Second, VPS35 in OBs is required for maintaining bone mass as well as PTH(1–34)-induced catabolic response. Third, PPP1R14C, an inhibitory subunit of PP1 phosphatase, interacts with not only VPS35, but also PTH1R; and it is involved in the activation of the non-canonical PTH1R signaling pathway and PTH(1–34)-induced catabolic response. Finally, our results support the view that PTH signaling events are closely coupled in time and spatial-dependent manners, which may be critical for PTH(1–34)-driven anabolic and catabolic responses.

The results that VPS35 interacts with PTH1R, and VPS35 is necessary for PTH(1–34)-induced PTH1R's endosome-to-Golgi translocation (Fig. 2), support the view for PTH1R as a cargo of VPS35/retromer not only in HEK293 cells (Feinstein et al., 2011), but also in OB-lineage cells. Interestingly, both PTH1R-VPS35 interaction and VPS35-mediated PTH1R's endosome-to-Golgi translocation were increased by PTH(1–34) stimulation (Fig. 2). Such endosome-to-Golgi translocation of PTH1R is time-dependent, which appears to be crucial for preventing PTH1R degradation as well as turning off PTH1R signaling. The latter view is in agreement with recent reports that retromer terminates not only PTH-,

but also vasopressin-induced increase of cAMP in HEK 293 cells (Feinstein et al., 2011; Feinstein et al., 2013). In addition to suppress these GPCR signaling, VPS35/retromer also inhibits RANK signaling in macrophages likely by promoting RANK endosome to Golgi translocation (Xia et al., 2013b). In aggregate, VPS35/retromer regulates GPCR-family receptors' trafficking, and VPS35/retromer-mediated endosome-to-Golgi trafficking may be critical not only for retrieval of the receptors/cargos, but also for suppression of their signaling.

Note that whereas PTH1R signaling is enhanced and prolonged in Vps35-deficient cells, PTH1R's degradation was accelerated. These results seem discrepant, but they are likely to be linked. Note that the time course for signaling studies (within 1-h) is shorter than those for protein degradation assays (1 to 8 h). It is possible that when the receptor (PTH1R) signaling is constitutively activated due to Vps35/retromer-deficiency, PTH1R's degradation machinery is thus turning on to prevent further activation of its down-stream signaling events. This view is in agreement with the notion for two cellular mechanisms to terminate a receptor signaling: one (a reversible/physiological one) is positively regulated by VPS35/retromer, and the other one (receptor degradation, an irreversible mechanism) is negatively regulated by VPS35/retromer.

How does VPS35/retromer turn off PTH1R signaling? Here we propose a working model that is depicted in Fig. 10F. In this model, VPS35/
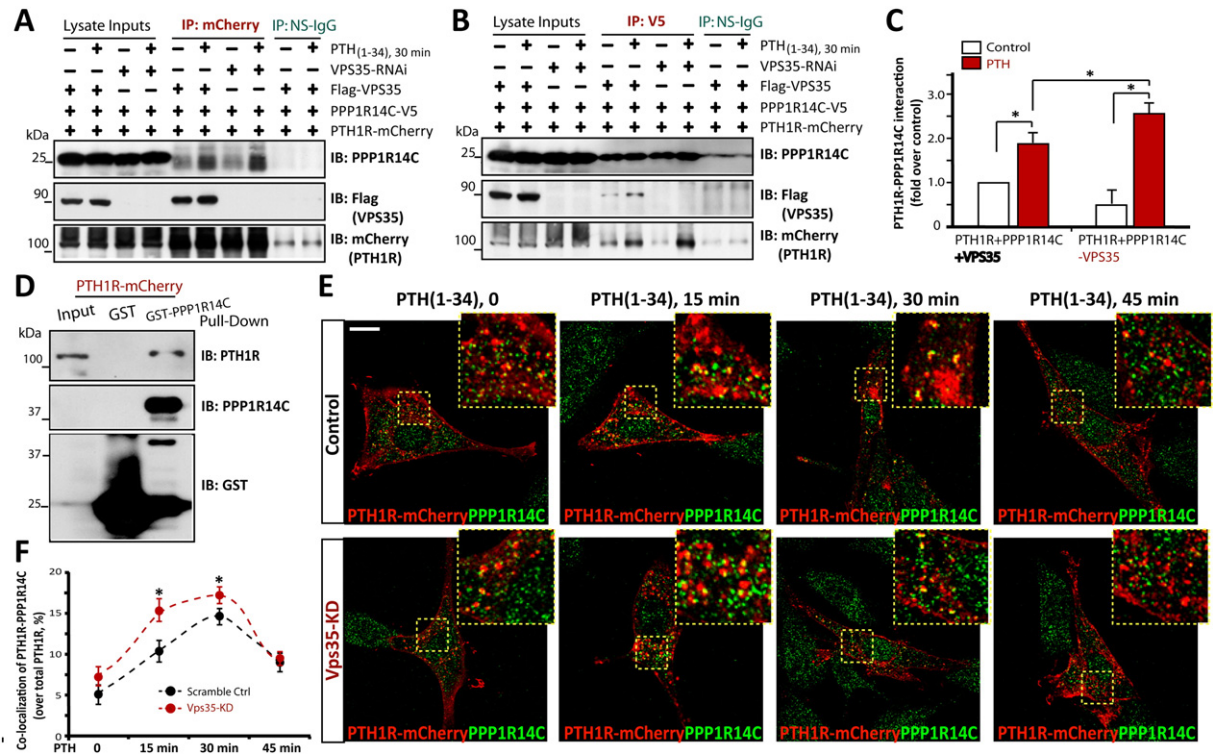
Fig. 8. PTH1R interaction with PPP1R14C. (A-C) Co-immunoprecipitation of PTH1R- PPP1R14C complex in the presence or absence of VPS35. HEK293T cells were transfected with indicated plasmids. 48 h post transfection, cells were treated with or without PTH$_{(1-34)}$(100 nM) for 30 min. Cell lysates were immunoprecipitated with *anti*-V5 (for PPP1R14C) or anti-mCherry (for PTH1R) antibodies, respectively. The resulting precipitates were subjected to immunoblotting analysis using indicated antibodies. The data presented are representative blots of 3-independent experiments. Quantification analyses were shown in C. (D) In vitro GST pull down assay using indicated GST fusion proteins was carried out in HEK293 lysates expressing PTH1R-mCherry. The precipitates associated with the GST beads were subjected to the Western blot analysis using indicated antibodies. (E–F) Co-localization of PTH1R with PPP1R14C in MC3T3 cells in the presence or absence of VPS35. MC3T3 cells were co-transfected with indicated plasmids. 48 h post transfection, cells were stimulated with PTH$_{(1-34)}$(100 nM) for the indicated time, and then subjected to the immunostaining analysis with indicated antibodies. Representative images were shown, and images marked with white squares were amplified and shown in right top corners. Quantification analyses of the optical intensity for the co-localization of PTH1R-PPP1R14C over total PTH1R were presented in E. Bar, 10 μm. The values of mean ± SD ($n = 25$ cells from 3-different experiments) were shown. *, $P < 0.05$, significant difference.

retromer interacts with PPP1R14C and reduces PTH$_{(1-34)}$-induced PTH1R-PPP1R14C complex, thus, allowing PP1 phosphatase to dephosphorylate the downstream signaling proteins, in particular, the endosomal signaling pathway, such as pCREB, pErk1/2, and pAkt (Fig. 9F). This model is in line with the following observations. PPP1R14C, an inhibitory subunit of PP1, forms complex with both VPS35/retromer (Fig. 7) and PTH1R (Fig. 8). Although both complex (VPS35-PPP1R14C and PTH1R-PPP1R14C) were stimulated by PTH$_{(1-34)}$ (Figs. 7-8), PTH1R-PPP1R14C complex appears to be negatively regulated by VPS35 (Fig. 8), implicating that both VPS35/retromer and PTH1R may compete for the interaction with PPP1R14C. PPP1R14C appears to selectively promote PTH1R-mediated endosomal, but not cell surface, signaling. By interacting with PPP1R14C, VPS35/retromer may terminate PTH's endosomal signaling by reducing PPP1R14C binding with PTH1R, releasing PPP1R14C's inhibitory effect on PP1 phosphatase, and thus enhancing PP1-driven dephosphorylations of endosomal signaling proteins (e.g., pErk1/2, pAkt, and pCREB)(Fig. 9F). When VPS35 is depleted, PPP1R14C may be largely in association with PTH1R complex in endosomes, where it could suppress PP1-mediated de-phosphorylations, and thus enhancing/sustaining PTH$_{(1-34)}$-driven endosomal/non-canonical phosphorylation events (Fig. 9F). It is of interest to note that PPP4C, a catalytic subunit of phosphatase, is also found to be involved in endosome-to-Golgi retrieval of membrane proteins (Borroni et al., 2014).

What is the functional significance of VPS35/retromer-turning off PTH1R signaling? The increased and sustained PTH$_{(1-34)}$ signaling in Vps35-deficient OB-lineage cells corroborates well with the impaired PTH$_{(1-34)}$-driven catabolic response (e.g., RANKL/OPG-expression and OC genesis). Suppression of PPP1R14C expression diminished not only the sustained endosomal PTH$_{(1-34)}$ signaling, but also the impaired catabolic response due to VPS35-deficiency (Figs. 9-10). These

observations lead to the speculation that VPS35/retromer turning off the endosomal PTH$_{(1-34)}$ signaling may be critical for PTH$_{(1-34)}$-induced catabolic response and bone remodeling, thus preventing a large bone-gain response. It is noteworthy that our results for PTH$_{(1-34)}$ responses in Vps35-deficient cells/mice are remarkably similar to that described for β-arrestin-biased ligand (D-Trp12,Tyr34)-PTH$_{(7-34)}$'s effect, which stimulates PTH1R-mediated endosomal/non-canonical β-arrestin signaling, promotes anabolic bone formation, but suppresses catabolic bone resorption (Gesty-Palmer et al., 2009; Whalen et al., 2011). It is also of interest to note that β-arrestins prolong rather than attenuate cAMP signaling triggered by GPCRs, including PTH1R and vasopressin receptor (van der Lee et al., 2013; Vilardaga et al., 2012; Whalen et al., 2011). Such β-arrestin mediated signaling is believed to be a non-canonical or endosomal signaling, as it is different from that of canonical or cell surface model. In the cell surface model, β-arrestin is thought to desensitize GPCR signaling at the plasma membrane by physically interacting with activated GPCR, such as rhodopsin and the β2-AR (Whalen et al., 2011). Another intriguing observation is that the structures of β-arrestins and the Vps26 subunit of retromer have a striking resemblance (Collins et al., 2008). Although the functional significance of this similarity remains unknown, it is possible that via VPS26, VPS35/retromer may complete with β-arrestin2 in binding to PTH1R in endosomes, thus, suppresses β-arrestin mediated non-canonical signaling. While this alternative hypothesis is of interest, it requires additional investigations.

In summary, the data presented in this manuscript demonstrate a critical function of VPS35 in regulating PTH1R trafficking. This event and VPS35-interaction with PPP1R14C appear to be essential for turning off PTH1R's endosomal signaling, and promoting PTH1R-mediated catabolic response and bone remodeling.
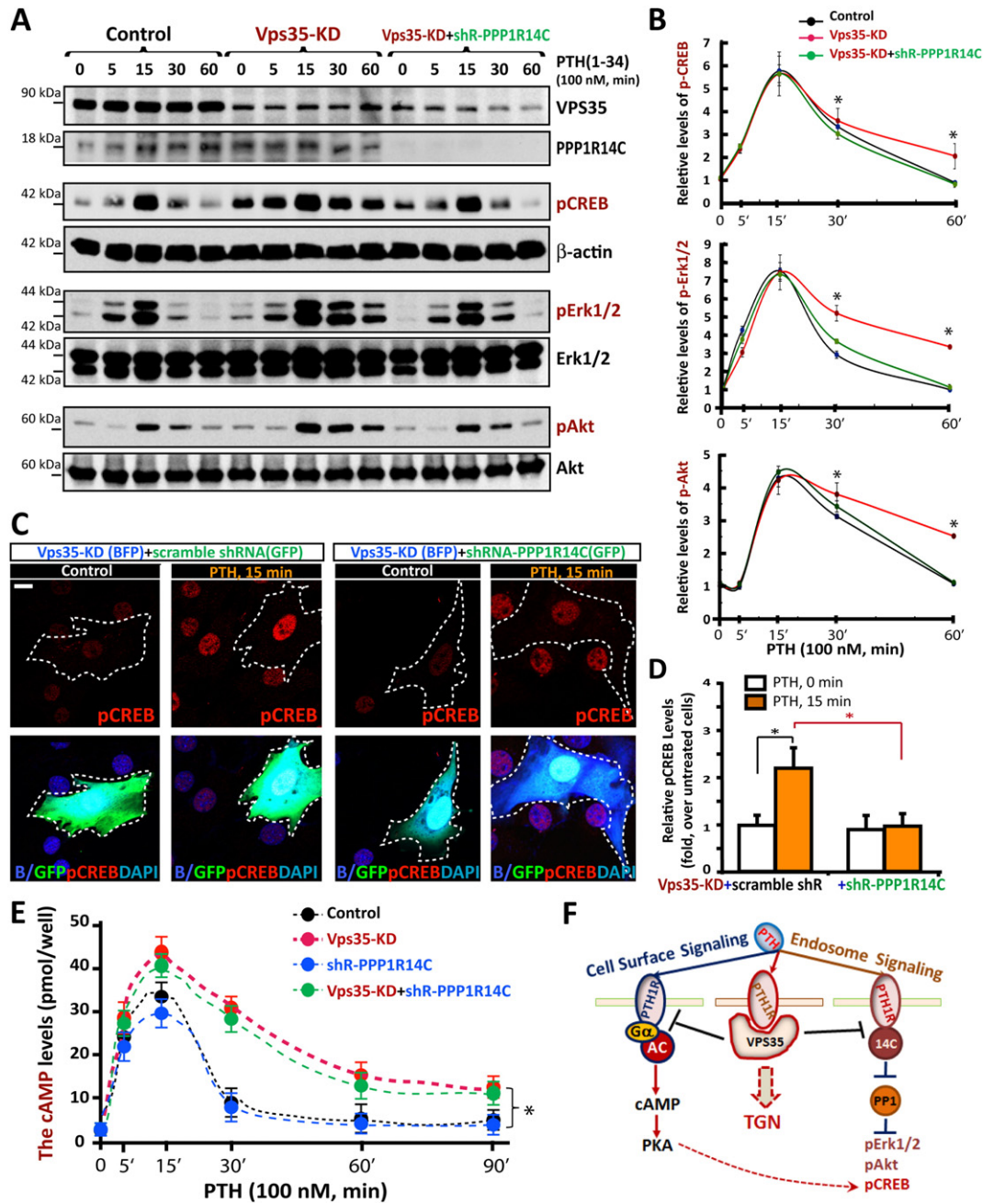
Fig. 9. Requirement of PPP1R14C for the enhanced PTH$_{(1–34)}$-driven endosomal signaling in Vps35-KD MC3T3 cells. (A-B) Western blot analysis of PTH$_{(1–34)}$-driven signaling in Control, Vps35-KD and Vps35-KD plus PPP1R14C-KD MC3T3 cells. Representative blots from 3-independent experiments were shown in A. The data were quantified by ImageJ software and presented in B as mean ± SD. *, $P < 0.05$. (C–D) Immunostaining analysis of pCREB in Vps35-KD and Vps35-KD plus PPP1R14C-KD MC3T3 cells treated with or without PTH$_{(1–34)}$ for 15 min. Representative images were shown in C. The pCREB levels in transfected cells (marked by BFP/GFP with dashed lines) were normalized to un-transfected cells in the same field of view. The quantification analyses shown in (D) were mean ± SD ($n = 30$ cells from 3-different assays). *, $P < 0.05$. Bar, 10 μm. (E) ELISA analysis of cAMP production in Control, Vps35-KD and Vps35-KD plus PPP1R14C-KD MC3T3 cells. Cells were serum starved overnight and stimulated with PTH$_{(1–34)}$(100 nM) for the indicated time in E. Then, cells were lysed with 0.1 M HCl and centrifuged, the supernatant were assayed by using a cAMP ELISA kit. (F) Illustration of a working model for a possible role of VPS35-PPP1R14C interaction in regulating PTH signaling.

Supplementary data to this article can be found online at http://dx.doi.org/10.1016/j.ebiom.2016.05.028.

Author Contributions

W.–C.X. and L.X. designed research; L.X. performed experiments in Figs. 1-10; W.-F.X. established primary BMSCs cultures; L.X. and F.-L.T. contributed reagents/plasmids; J.-X.P. assisted in cell culture; W.–C.X., L.X. and L.M. analyzed data; W.–C.X. and L.X. wrote the paper.

Conflict of Interest Statement

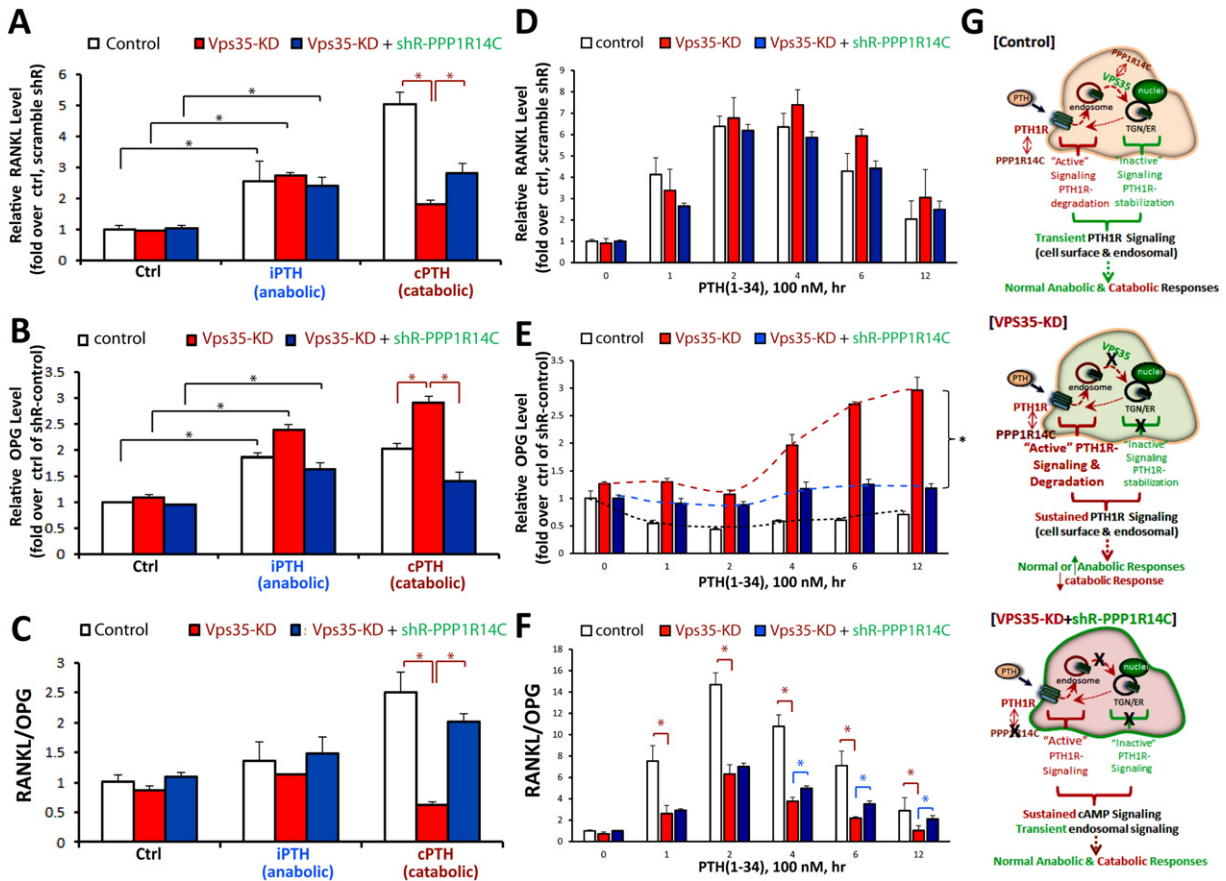The authors declare that they have no conflicts of interest.

Fig. 10. Diminished deficit in PTH$_{(1-34)}$-induced catabolic response in Vps35-KD MC3T3 cells suppressing PPP1R14C's expression. (A–F) Real-time PCR analysis of the mRNA levels of RANKL, and OPG in control (scramble shRNA), Vps35-KD plus scramble shR, and Vps35-KD plus shR-PPP1R14C MC3T3 cells in response to indicated PTH$_{(1-34)}$ stimulations. In (A–C), cells were treated with Ctrl (PBS), iPTH (100 nM, 1-h per day for 6 days), or cPTH (100 nM, daily change with fresh medium containing PTH$_{(1-34)}$) as described in Method and Fig. 4A. In (D–F), cells were treated with PTH$_{(1-34)}$(100 nM) for indicated time. The values are normalized to β-actin. Ratio of RANKL/OPG was shown in C and F. The values of mean ± SD from 3-different experiments were presented. *, $p < 0.05$. (G) Illustration of working models for VPS35 and PPP1R14C to differentially regulate PTH1R cell surface and endosomal signaling dynamics and function.

References

Belenkaya, T.Y., Wu, Y., Tang, X., Zhou, B., Cheng, L., Sharma, Y.V., Yan, D., Selva, E.M., Lin, X., 2008. The retromer complex influences Wnt secretion by recycling wntless from endosomes to the *trans*-Golgi network. Dev. Cell 14, 120–131.

Bonifacino, J.S., Hurley, J.H., 2008. Retromer. Curr. Opin. Cell Biol. 20, 427–436.

Borroni, B., Ferrari, F., Galimberti, D., Nacmias, B., Barone, C., Bagnoli, S., Fenoglio, C., Piaceri, I., Archetti, S., Bonvicini, C., et al., 2014. Heterozygous TREM2 mutations in frontotemporal dementia. Neurobiol. Aging 35 (934) (e937-910).

Cheloha, R.W., Gellman, S.H., Vilardaga, J.P., Gardella, T.J., 2015. PTH receptor-1 signalling-mechanistic insights and therapeutic prospects. Nat. Rev. Endocrinol. 11, 712–724.

Chen, D., Xiao, H., Zhang, K., Wang, B., Gao, Z., Jian, Y., Qi, X., Sun, J., Miao, L., Yang, C., 2010. Retromer is required for apoptotic cell clearance by phagocytic receptor recycling. Science 327, 1261–1264.

Choy, R.W., Park, M., Temkin, P., Herring, B.E., Marley, A., Nicoll, R.A., von Zastrow, M., 2014. Retromer mediates a discrete route of local membrane delivery to dendrites. Neuron 82, 55–62.

Collins, B.M., Norwood, S.J., Kerr, M.C., Mahony, D., Seaman, M.N., Teasdale, R.D., Owen, D.J., 2008. Structure of Vps26B and mapping of its interaction with the retromer protein complex. Traffic 9, 366–379.

Coudreuse, D.Y., Roel, G., Betist, M.C., Destree, O., Korswagen, H.C., 2006. Wnt gradient formation requires retromer function in Wnt-producing cells. Science 312, 921–924.

Cui, S., Xiong, F., Hong, Y., Jung, J.U., Li, X.S., Liu, J.Z., Yan, R., Mei, L., Feng, X., Xiong, W.C., 2010. APPswe/Abeta regulation of osteoclast activation and RAGE expression in an age dependent manner. J. Bone Miner. Res. 26, 1084–1098.

Dhungel, N., Eleuteri, S., Li, L.B., Kramer, N.J., Chartron, J.W., Spencer, B., Kosberg, K., Fields, J.A., Stafa, K., Adame, A., et al., 2015. Parkinson's disease genes VPS35 and EIF4G1 interact genetically and converge on alpha-synuclein. Neuron 85, 76–87.

Drgonova, J., Zimonjic, D.B., Hall, F.S., Uhl, G.R., 2010. Effect of KEPI (Ppp1r14c) deletion on morphine analgesia and tolerance in mice of different genetic backgrounds: when a knockout is near a relevant quantitative trait locus. Neuroscience 165, 882–895.

Duong, L.T., Lakkakorpi, P.T., Nakamura, I., Machwate, M., Nagy, R.M., Rodan, G.A., 1998. PYK2 in osteoclasts is an adhesion kinase, localized in the sealing zone, activated by ligation of alpha(v)beta3 integrin, and phosphorylated by src kinase. J. Clin. Invest. 102, 881–892.

Eaton, S., 2008. Retromer retrieves wntless. Dev. Cell 14, 4–6.

Eto, M., 2009. Regulation of cellular protein phosphatase-1 (PP1) by phosphorylation of the CPI-17 family, C-kinase-activated PP1 inhibitors. J. Biol. Chem. 284, 35273–35277.

Feinstein, T.N., Wehbi, V.L., Ardura, J.A., Wheeler, D.S., Ferrandon, S., Gardella, T.J., Vilardaga, J.P., 2011. Retromer terminates the generation of cAMP by internalized PTH receptors. Nat. Chem. Biol. 7, 278–284.

Feinstein, T.N., Yui, N., Webber, M.J., Wehbi, V.L., Stevenson, H.P., King Jr., J.D., Hallows, K.R., Brown, D., Bouley, R., Vilardaga, J.P., 2013. Noncanonical control of vasopressin receptor type 2 signaling by retromer and arrestin. J. Biol. Chem. 288, 27849–27860.

Franch-Marro, X., Wendler, F., Guidato, S., Griffith, J., Baena-Lopez, A., Itasaki, N., Maurice, M.M., Vincent, J.P., 2008. Wingless secretion requires endosome-to-Golgi retrieval of Wntless/Evi/Sprinter by the retromer complex. Nat. Cell Biol. 10, 170–177.

Fu, Q., Jilka, R.L., Manolagas, S.C., O'Brien, C.A., 2002. Parathyroid hormone stimulates receptor activator of NFkappa B ligand and inhibits osteoprotegerin expression via protein kinase A activation of cAMP-response element-binding protein. J. Biol. Chem. 277, 48868–48875.

Gesty-Palmer, D., Flannery, P., Yuan, L., Corsino, L., Spurney, R., Lefkowitz, R.J., Luttrell, L.M., 2009. A beta-arrestin-biased agonist of the parathyroid hormone receptor (PTH1R) promotes bone formation independent of G protein activation. Sci. Transl. Med. 1, 1ra1.

Guerreiro, R., Bras, J., Hardy, J., 2013. SnapShot: genetics of Alzheimer's disease. Cell 155, 968--9968 (e961).

Helfrich, M.H., Hocking, L.J., 2008. Genetics and aetiology of Pagetic disorders of bone. Arch. Biochem. Biophys. 473, 172–182.

Huang, J.C., Sakata, T., Pfleger, L.L., Bencsik, M., Halloran, B.P., Bikle, D.D., Nissenson, R.A., 2004. PTH differentially regulates expression of RANKL and OPG. J. Bone Miner. Res. 19, 235–244.

Issack, P.S., Lauerman, M.H., Helfet, D.L., Doty, S.B., Lane, J.M., 2007. Alendronate inhibits PTH (1-34)-induced bone morphogenetic protein expression in MC3T3-E1 preosteoblastic cells. HSS J. 3, 169–172.

Liu, Q.R., Zhang, P.W., Zhen, Q., Walther, D., Wang, X.B., Uhl, G.R., 2002. KEPI, a PKC-dependent protein phosphatase 1 inhibitor regulated by morphine. J. Biol. Chem. 277, 13312–13320.

Liu, Y., Peng, Y., Dai, P.G., Du, Q.S., Mei, L., Xiong, W.C., 2012. Differential regulation of myosin X movements by its cargos, DCC and neogenin. J. Cell Sci. 125, 751–762.

Luckhaus, C., Mahabadi, B., Grass-Kapanke, B., Janner, M., Willenberg, H., Jager, M., Supprian, T., Fehsel, K., 2009. Blood biomarkers of osteoporosis in mild cognitive impairment and Alzheimer's disease. J. Neural Transm. 116, 905–911.

McGough, I.J., Cullen, P.J., 2011. Recent advances in retromer biology. Traffic 12, 963–971.

Melton 3rd, L.J., Beard, C.M., Kokmen, E., Atkinson, E.J., O'Fallon, W.M., 1994. Fracture risk in patients with Alzheimer's disease. J. Am. Geriatr. Soc. 42, 614–619.

Moriya, S., Hayata, T., Notomi, T., Aryal, S., Nakamaoto, T., Izu, Y., Kawasaki, M., Yamada, T., Shirakawa, J., Kaneko, K., et al., 2015. PTH regulates beta2-adrenergic receptor expression in osteoblast-like MC3T3-E1 cells. J. Cell. Biochem. 116, 142–148.

Muhammad, A., Flores, I., Zhang, H., Yu, R., Staniszewski, A., Planel, E., Herman, M., Ho, L., Kreber, R., Honig, L.S., et al., 2008. Retromer deficiency observed in Alzheimer's disease causes hippocampal dysfunction, neurodegeneration, and Abeta accumulation. Proc. Natl. Acad. Sci. U. S. A. 105, 7327–7332.

Paloneva, J., Mandelin, J., Kiialainen, A., Bohling, T., Prudlo, J., Hakola, P., Haltia, M., Konttinen, Y.T., Peltonen, L., 2003. DAP12/TREM2 deficiency results in impaired osteoclast differentiation and osteoporotic features. J. Exp. Med. 198, 669–675.

Pan, C.L., Baum, P.D., Gu, M., Jorgensen, E.M., Clark, S.G., Garriga, G., 2008. C. elegans AP-2 and retromer control Wnt signaling by regulating mig-14/Wntless. Dev. Cell 14, 132–139.

Pfaff, M., Jurdic, P., 2001. Podosomes in osteoclast-like cells: structural analysis and cooperative roles of paxillin, proline-rich tyrosine kinase 2 (Pyk2) and integrin alphaVbeta3. J. Cell Sci. 114, 2775–2786.

Reid, I.R., 2012. Pharmacotherapy of Paget's disease of bone. Expert. Opin. Pharmacother. 13, 637–646.

Sato, Y., Asoh, T., Oizumi, K., 1998. High prevalence of vitamin D deficiency and reduced bone mass in elderly women with Alzheimer's disease. Bone 23, 555–557.

Sato, Y., Kanoko, T., Satoh, K., Iwamoto, J., 2004. Risk factors for hip fracture among elderly patients with Alzheimer's disease. J. Neurol. Sci. 223, 107–112.

Schiller, P.C., D'Ippolito, G., Roos, B.A., Howard, G.A., 1999. Anabolic or catabolic responses of MC3T3-E1 osteoblastic cells to parathyroid hormone depend on time and duration of treatment. J. Bone Miner. Res. 14, 1504–1512.

Seaman, M.N., 2004. Cargo-selective endosomal sorting for retrieval to the Golgi requires retromer. J. Cell Biol. 165, 111–122.

Seaman, M.N., 2005. Recycle your receptors with retromer. Trends Cell Biol. 15, 68–75.

Seaman, M.N., Marcusson, E.G., Cereghino, J.L., Emr, S.D., 1997. Endosome to Golgi retrieval of the vacuolar protein sorting receptor, Vps10p, requires the function of the VPS29, VPS30, and VPS35 gene products. J. Cell Biol. 137, 79–92.

Seaman, M.N., Gautreau, A., Billadeau, D.D., 2013. Retromer-mediated endosomal protein sorting: all WASHed up! Trends Cell Biol. 23, 522–528.

Simmonds, C.S., Kovacs, C.S., 2010. Role of parathyroid hormone (PTH) and PTH-related protein (PTHrP) in regulating mineral homeostasis during fetal development. Crit. Rev. Eukaryot. Gene Expr. 20, 235–273.

Singaraja, R.R., 2013. TREM2: a new risk factor for Alzheimer's disease. Clin. Genet. 83, 525–526.

Small, S.A., Petsko, G.A., 2015. Retromer in Alzheimer disease, Parkinson disease and other neurological disorders. Nat. Rev. Neurosci. 16, 126–132.

Small, S.A., Kent, K., Pierce, A., Leung, C., Kang, M.S., Okada, H., Honig, L., Vonsattel, J.P., Kim, T.W., 2005. Model-guided microarray implicates the retromer complex in Alzheimer's disease. Ann. Neurol. 58, 909–919.

Tabuchi, M., Yanatori, I., Kawai, Y., Kishi, F., 2010. Retromer-mediated direct sorting is required for proper endosomal recycling of the mammalian iron transporter DMT1. J. Cell Sci. 123, 756–766.

Tan, Z.S., Seshadri, S., Beiser, A., Zhang, Y., Felson, D., Hannan, M.T., Au, R., Wolf, P.A., Kiel, D.P., 2005. Bone mineral density and the risk of Alzheimer disease. Arch. Neurol. 62, 107–111.

Tang, F.L., Erion, J.R., Tian, Y., Liu, W., Yin, D.M., Ye, J., Tang, B., Mei, L., Xiong, W.C., 2015a. VPS35 in dopamine neurons is required for endosome-to-Golgi retrieval of Lamp2a, a receptor of chaperone-mediated autophagy that is critical for alpha-synuclein degradation and prevention of pathogenesis of Parkinson's disease. J. Neurosci. 35, 10613–10628.

Tang, F.L., Liu, W., Hu, J.X., Erion, J.R., Ye, J., Mei, L., Xiong, W.C., 2015b. VPS35 deficiency or mutation causes dopaminergic neuronal loss by impairing mitochondrial fusion and function. Cell Rep. 12, 1631–1643.

Temkin, P., Lauffer, B., Jager, S., Cimermancic, P., Krogan, N.J., von Zastrow, M., 2011. SNX27 mediates retromer tubule entry and endosome-to-plasma membrane trafficking of signalling receptors. Nat. Cell Biol. 13, 715–721.

Tysiewicz-Dudek, M., Pietraszkiewicz, F., Drozdzowska, B., 2008. Alzheimer's disease and osteoporosis: common risk factors or one condition predisposing to the other? Ortop. Traumatol. Rehabil. 10, 315–323.

van der Lee, M.M.C., Verkaar, F., Wat, J.W.Y., van Offenbeek, J., Timmerman, M., Voorneveld, L., van Lith, L.H.C.J., Zaman, G.J.R., 2013. Beta-arrestin-biased signaling of PTH analogs of the type 1 parathyroid hormone receptor. Cell. Signal. 25, 527–538.

Vieira, S.I., Rebelo, S., Esselmann, H., Wiltfang, J., Lah, J., Lane, R., Small, S.A., Gandy, S., da Cruz, E.S.E.F., da Cruz, E.S.O.A., 2010. Retrieval of the Alzheimer's amyloid precursor protein from the endosome to the TGN is S655 phosphorylation state-dependent and retromer-mediated. Mol. Neurodegener. 5, 40.

Vilardaga, J.P., Gardella, T.J., Wehbi, V.L., Feinstein, T.N., 2012. Non-canonical signaling of the PTH receptor. Trends Pharmacol. Sci. 33, 423–431.

Vilarino-Guell, C., Wider, C., Ross, O.A., Dachsel, J.C., Kachergus, J.M., Lincoln, S.J., Soto-Ortolaza, A.I., Cobb, S.A., Wilhoite, G.J., Bacon, J.A., et al., 2011. VPS35 mutations in Parkinson disease. Am. J. Hum. Genet. 89, 162–167.

Wang, Q., Xie, Y., Du, Q.S., Wu, X.J., Feng, X., Mei, L., McDonald, J.M., Xiong, W.C., 2003. Regulation of the formation of osteoclastic actin rings by proline-rich tyrosine kinase 2 interacting with gelsolin. J. Cell Biol. 160, 565–575.

Wang, C.L., Tang, F.L., Peng, Y., Shen, C.Y., Mei, L., Xiong, W.C., 2012. VPS35 regulates developing mouse hippocampal neuronal morphogenesis by promoting retrograde trafficking of BACE1. Biol. Open 1, 1248–1257.

Wen, L., Tang, F.L., Hong, Y., Luo, S.W., Wang, C.L., He, W., Shen, C., Jung, J.U., Xiong, F., Lee, D.H., et al., 2011. VPS35 haploinsufficiency increases Alzheimer's disease neuropathology. J. Cell Biol. 195, 765–779.

Wenzel, K., Daskalow, K., Herse, F., Seitz, S., Zacharias, U., Schenk, J.A., Schulz, H., Hubner, N., Micheel, B., Schlag, P.M., et al., 2007. Expression of the protein phosphatase 1 inhibitor KEPI is downregulated in breast cancer cell lines and tissues and involved in the regulation of the tumor suppressor EGR1 via the MEK-ERK pathway. Biol. Chem. 388, 489–495.

Whalen, E.J., Rajagopal, S., Lefkowitz, R.J., 2011. Therapeutic potential of beta-arrestin- and G protein-biased agonists. Trends Mol. Med. 17, 126–139.

Xia, W.F., Jung, J.U., Shun, C., Xiong, L., Shi, X.M., Mei, L., Xiong, W.C., 2013a. Swedish mutant APP suppresses osteoblast differentiation and causes osteoporotic deficit, which are ameliorated by n-acetyl-l-cysteine. J. Bone Miner. Res. 28, 2122–2135.

Xia, W.F., Tang, F.L., Xiong, L., Xiong, S., Jung, J.U., Lee, D.H., Li, X.S., Feng, X., Mei, L., Xiong, W.C., 2013b. Vps35 loss promotes hyperresorptive osteoclastogenesis and osteoporosis via sustained RANKL signaling. J. Cell Biol. 200, 821–837.

Yang, P.T., Lorenowicz, M.J., Silhankova, M., Coudreuse, D.Y., Betist, M.C., Korswagen, H.C., 2008. Wnt signaling requires retromer-dependent recycling of MIG-14/Wntless in Wnt-producing cells. Dev. Cell 14, 140–147.

Zhong, Z., Zylstra-Diegel, C.R., Schumacher, C.A., Baker, J.J., Carpenter, A.C., Rao, S., Yao, W., Guan, M., Helms, J.A., Lane, N.E., et al., 2012. Wntless functions in mature osteoblasts to regulate bone mass. Proc. Natl. Acad. Sci. U. S. A. 109, E2197–E2204.

Zhou, Z., Immel, D., Xi, C.X., Bierhaus, A., Feng, X., Mei, L., Nawroth, P., Stern, D.M., Xiong, W.C., 2006. Regulation of osteoclast function and bone mass by RAGE. J. Exp. Med. 203, 1067–1080.

Zhou, Z., Han, J.Y., Xi, C.X., Xie, J.X., Feng, X., Wang, C.Y., Mei, L., Xiong, W.C., 2008. HMGB1 regulates RANKL-induced osteoclastogenesis in a manner dependent on RAGE. J. Bone Miner. Res. 23, 1084–1096.

Zhu, X.J., Wang, C.Z., Dai, P.G., Xie, Y., Song, N.N., Liu, Y., Du, Q.S., Mei, L., Ding, Y.Q., Xiong, W.C., 2007. Myosin X regulates netrin receptors and functions in axonal path-finding. Nat. Cell Biol. 9, 184–192.

Zimprich, A., Benet-Pages, A., Struhal, W., Graf, E., Eck, S.H., Offman, M.N., Haubenberger, D., Spielberger, S., Schulte, E.C., Lichtner, P., et al., 2011. A mutation in VPS35, encoding a subunit of the retromer complex, causes late-onset Parkinson disease. Am. J. Hum. Genet. 89, 168–175.